NATIONAL ADVISORY COMMITTEE FOR AERONAUTICS

TECHNICAL NOTE 3619

EFFECT OF CARRIAGE MASS UPON THE LOADS AND MOTIONS OF A PRISMATIC BODY DURING HYDRODYNAMIC IMPACT

By Melvin F. Markey

Langley Aeronautical Laboratory
Langley Field, Va.

Washington
March 1956

B

NATIONAL ADVISORY COMMITTEE FOR AERONAUTICS

TECHNICAL NOTE 3619

EFFECT OF CARRIAGE MASS UPON THE LOADS AND MOTIONS OF A PRISMATIC BODY DURING HYDRODYNAMIC IMPACT

By Melvin F. Markey

SUMMARY

A theoretical derivation for the effect of a towing-carriage mass upon the general equations of motion is made for a prismatic body during a hydrodynamic impact. The resulting equations include a correction factor j that depends on the trim and the ratio of the carriage mass to the body mass. The equations can be used at any stage of the impact to determine the resulting loads and motions of the body, including the effect of a carriage mass.

Because of the complexity of the equations for the completely general case, it is necessary to choose examples to aid in showing the conditions at which the carriage mass is important. The examples chosen are the V-bottom float with nonimmersed chines and the flat plate with deeply immersed chines. For these examples the equations are analyzed at particular stages of the impact, namely, at maximum acceleration and at maximum penetration. At these stages indicative curves are plotted for an infinite carriage mass in one case and with the carriage mass neglected in another. The difference between the two curves shows the maximum possible effect of the carriage mass at the stages selected.

The curves indicate that for the V-bottom float with nonimmersed chines the carriage-mass effect is more pronounced at high trims. At low approach parameters and high trims, a carriage mass is found to have an effect on all the coefficients investigated. At the high approach parameters and high trims, the effect of carriage mass on the vertical-velocity ratio, acceleration, and pitching-moment coefficients is noticeable. At a trim of 15° and an approach parameter equal to or greater than 1.0 (flight-path angle $\leq 13^\circ$), the maximum percentage change in any of the coefficients investigated at the particular stages selected is about 10 percent or less because of carriage-mass effect.

The maximum percentage change in the maximum penetration and maximum acceleration due to a carriage mass is of the same order for the V-bottom float with nonimmersed chines and the flat plate with deeply immersed chines at flight-path angles of 2.5°, 5.5°, 10°, and 20° and trims of 15°, 30°, and 45° for beam loadings from 1 to 100.

INTRODUCTION

Theories have been published regarding the loads and motions of prismatic bodies during hydrodynamic impacts for both immersed chines and nonimmersed chines. For these theories, however, a free-body impact is assumed, whereas for some experimental testing facilities a restraint is imposed in the horizontal direction by a towing-carriage mass. Therefore, questions have arisen concerning the importance of carriage-mass effect upon the results obtained, since errors in the results might lead to erroneous conclusions in testing programs.

The carriage mass is expected to have little effect for the low trims, since at this condition the resisting water force has only a small component in the horizontal direction. However, for the higher trims, at which some modern seaplanes may operate and at which tests may be conducted, the effect is not known.

The purpose of the present investigation is to determine the effect of carriage mass upon the general theoretical equations of motion for the prismatic body during a hydrodynamic impact and to indicate under what conditions the effect is important. The derivations are analogous to those of the free-body impacts of the references 1 to 4, the only difference being the inclusion of a factor that depends on carriage mass and trim. General expressions applicable to any prismatic body are obtained for the loads and motions during impact, and curves are presented to aid in showing the conditions at which the carriage-mass effect is important.

SYMBOLS

a	resultant acceleration
B	Bobyleff's flow coefficient
b	beam of hull at chines
C_L	impact lift coefficient, $\frac{-\ddot{z}W}{\frac{1}{2}\rho g b^2 V_o^2}$
C_Δ	beam-loading coefficient, $\frac{W}{\rho g b^3}$
j	carriage-mass correction factor
F	resultant hydrodynamic force

g	acceleration due to gravity
G	corrected approach parameter, $\frac{\kappa + 1 - j}{j}$
J_1	three-dimensional mass parameter
k_1	penetration parameter
l	wetted length along keel
m_w	two-dimensional water mass in transverse plane
M	pitching moment, positive nose up
Q_1	velocity parameter
s	distance from foremost immersed station along keel to flow plane
t	time after water contact
V	velocity
W	weight
x	distance parallel to undisturbed water surface, positive in direction of float motion
$\dot{x}$	horizontal velocity of float
$\ddot{x}$	horizontal acceleration of float
z	immersion of keel at step normal to undisturbed water surface, positive downward
$\dot{z}$	vertical velocity of float
$\ddot{z}$	vertical acceleration of float
β	angle of dead rise
$f(\beta)$	dead-rise function
γ	flight-path angle
ζ	distance from keel to undisturbed water surface in any given flow plane, normal to keel, positive downward

$\dot{\zeta}$ velocity of float normal to keel

$\ddot{\zeta}$ acceleration of float normal to keel

ζ' immersion of keel normal to itself into a flow plane, corrected for water rise at keel

$\dot{\zeta}'$ partial derivative of ζ' with respect to time

θ angle between vertical and resultant acceleration

κ approach parameter for free-body landing, $\frac{\sin \tau}{\sin \gamma_o} \cos(\tau + \gamma_o)$

λ ratio of length of keel below undisturbed water surface to mean beam

λ' ratio of length of keel below elevated water surface to mean beam

ρ mass density of water

τ trim angle

$\varphi(\lambda)$ Pabst's aspect-ratio correction based on λ

$\varphi(\lambda')$ Pabst's aspect-ratio correction based on λ'

$\varphi_1(\lambda)$ pitching-moment aspect-ratio correction

Subscripts:

a direction perpendicular to resultant acceleration

b float

c carriage

o at water contact

γ resultant velocity

s at step

x horizontal direction

z vertical direction

ζ direction normal to keel

max maximum

Generalized variables:

m generalized pitching moment

p generalized center-of-pressure distance

u generalized displacement

u' generalized velocity

u" generalized acceleration

σ generalized time

THEORETICAL EQUATIONS OF MOTION

The case considered (shown in figs. 1(a) and (b)) consists of a float of effective weight W_b attached to a carriage of weight W_c. The float is free to move in the vertical direction, but it is constrained in the horizontal direction because of the influence of the carriage mass. The general equation of motion for the prismatic body during a hydrodynamic impact on a smooth water surface is formulated on the basis that flow occurs in transverse planes normal to the keel. The effects of viscosity, buoyancy, and changes in trim are neglected and a two-dimensional treatment with a three-dimensional aspect-ratio correction is made. (See refs. 1 and 2.)

The force of a particular flow plane upon the body is equated to its change of momentum with respect to time as follows:

$$dF_\zeta = \frac{\partial}{\partial t}\left(m_w \dot{\zeta}\right) ds \tag{1}$$

where m_w is the two-dimensional water mass affected, ds is an incremental distance along the wetted length, and $\dot{\zeta}$ is the velocity of the body normal to the keel.

Including a three-dimensional aspect-ratio correction factor $\varphi(\lambda')$ and integrating equation (1) over the wetted length of the body yields

$$F_\zeta = \varphi(\lambda') \int_0^l \frac{\partial}{\partial t} m_w \dot{\zeta}\, ds$$

$$= \varphi(\lambda') \left(\int_0^l \dot{\zeta} \frac{\partial m_w}{\partial t} ds + \ddot{\zeta} \int_0^l m_w\, ds \right) \tag{2}$$

The first integral on the right-hand side of equation (2) represents the part of the total force that can be associated with the planing of the body ($\ddot{\zeta} = 0$), and the second integral represents that part associated with the acceleration of the virtual mass, where the virtual mass is usually defined as

$$\int_0^l m_w\, ds$$

At this point it is only necessary to substitute the proper expressions into equation (2) to get the equation including the carriage-mass effect. For this purpose, the following relations are utilized:

$$F_\zeta = \sqrt{F_x^2 + F_z^2}$$

$$= F_z \sec \tau \tag{3}$$

where

$$F_x = - \frac{W_c + W_b}{g} \ddot{x} \tag{4a}$$

$$F_z = - \frac{W_b}{g} \ddot{z} \tag{4b}$$

The acceleration $\ddot{x}$ is positive in the direction of motion, and $\ddot{z}$ is positive downward (fig. 1).

The relation for the acceleration normal to the keel is given as follows:

$$\ddot{\zeta} = \ddot{x} \sin \tau + \ddot{z} \cos \tau \tag{5}$$

Using equations (4) to determine the relation between horizontal and vertical acceleration gives

$$\frac{\ddot{x}}{\ddot{z}} = \frac{W_b}{W_b + W_c} \frac{F_x}{F_z} \tag{6}$$

If θ is now defined as $\tan^{-1} \frac{\ddot{x}}{\ddot{z}}$ and $\tan \tau$ is substituted for F_x/F_z, equation (6) becomes

$$\tan \theta = \frac{W_b}{W_b + W_c} \tan \tau \tag{7}$$

Equation (7) shows that the angle θ remains a constant throughout the impact and depends only on the trim and the ratio of the carriage mass to the float mass. Equation (7) also shows that, when the carriage mass equals zero (the free-body case), $\tau = \theta$ and the resultant acceleration is then normal to the keel. If the carriage mass does not equal zero, the resultant acceleration is not normal to the keel but at an angle θ from the vertical (fig. 1).

Equations (3) and (4b) may be combined with equations (5) and (7) to give

$$F_\zeta = - \frac{W_b \ddot{\zeta}}{g} \left(\frac{1}{\cos^2 \tau + \frac{\sin^2 \tau}{1 + \frac{W_c}{W_b}}} \right) \tag{8}$$

Let

$$j = \cos^2 \tau + \frac{\sin^2 \tau}{1 + \frac{W_c}{W_b}} \tag{9}$$

Then equation (8) becomes

$$F_\zeta = - \frac{W_b \ddot{\zeta}}{gj} \tag{10}$$

Equation (10) may now be substituted into equation (2) to obtain

$$- \frac{W_b \ddot{\zeta}}{gj} = \varphi(\lambda') \left(\int_0^l \dot{\zeta} \frac{\partial m_w}{\partial t} \, ds + \ddot{\zeta} \int_0^l m_w \, ds \right) \tag{11}$$

The two-dimensional mass m_w for a given float is then assumed to be a function of the penetration normal to the keel; that is,

$$m_w = f(\zeta') \tag{12}$$

This function may be differentiated with respect to time to give

$$\frac{\partial m_w}{\partial t} = \frac{\partial m_w}{\partial \zeta'} \frac{\partial \zeta'}{\partial t} = \frac{\partial m_w}{\partial \zeta'} \dot{\zeta}' \tag{13}$$

Figure 1(b) shows that $s = \frac{\zeta'}{\tan \tau}$; therefore,

$$ds = \frac{d\zeta'}{\tan \tau} \tag{14}$$

Substituting equations (13) and (14) into equation (11) gives

$$-\frac{W_b \ddot{\zeta}}{gj} = \varphi(\lambda') \left(\int_0^{m_w, s} \frac{\dot{\zeta} \dot{\zeta}'}{\tan \tau} dm_w + \ddot{\zeta} \int_0^{l} m_w \, ds \right) \tag{15}$$

If the water rise at the keel is considered constant for the deeply immersed chine and is neglected for the nonimmersed chine,

$$\dot{\zeta} = \dot{\zeta}' \tag{16}$$

Substituting equation (16) into equation (15) gives

$$-\frac{W_b \ddot{\zeta}}{gj} = \varphi(\lambda') \left(\int_0^{m_w, s} \frac{\dot{\zeta}^2}{\tan \tau} dm_w + \ddot{\zeta} \int_0^{l} m_w \, ds \right) \tag{17}$$

In order to solve equation (17) in terms of the vertical components referred to the water surface, the following expressions are used:

$$\zeta_s = \frac{z}{\cos \tau} \tag{18}$$

$$\dot{\zeta} = \frac{V_a \sin \tau}{\cos \theta} + \dot{z}(\tan \theta \sin \tau + \cos \tau) \tag{19}$$

$$\ddot{\zeta} = \frac{j\ddot{z}}{\cos \tau} \tag{20}$$

Equation (19) is obtained from the equation

$$\dot{\zeta} = \dot{x} \sin \tau + \dot{z} \cos \tau$$

if $\dot{x}$ is eliminated by use of the relation

$$V_a = \dot{x} \cos \theta - \dot{z} \sin \theta$$

where V_a is the constant velocity during impact. Equation (20) is obtained from equations (5), (6), and (7).

Using equation (7) with (19) and (20), substituting into (17), and integrating gives the following expression, which applies at any instant of time:

$$\ddot{z}\left[1 + \frac{gj}{W_b} \varphi(\lambda') \int_0^l m_w \, ds\right] = - \frac{g m_{w,s} \varphi(\lambda')}{W_b \sin \tau}\left(j\dot{z} + \frac{V_a \sin \tau \cos \tau}{\cos \theta}\right)^2 \tag{21}$$

Rearranging equation (21) in integral form and using

$$\ddot{z} \, dz = \frac{d\dot{z}}{dt} dz = \dot{z} \, d\dot{z} \tag{22}$$

results in the following equation:

$$\frac{1}{j^2} \int_{\dot{z}_o}^{\dot{z}} \frac{\dot{z} \, d\dot{z}}{\left(\dot{z} + \frac{V_a \sin \tau \cos \tau}{j \cos \theta}\right)^2} = - \int_0^z \frac{\frac{m_{w,s}}{\sin \tau} dz}{\frac{W_b}{g\varphi(\lambda')} + j \int_0^l m_w \, ds} \tag{23}$$

Integration of equation (23) yields the following equation which expresses the velocity as a function of the penetration:

$$\frac{1}{j^2}\left(\log_e \frac{\frac{\dot{z}}{\dot{z}_o} + G}{1 + G} + \frac{G}{\frac{\dot{z}}{\dot{z}_o} + G} - \frac{G}{1 + G}\right) = - \int_0^z \frac{\frac{m_{w,s}}{\sin \tau} dz}{\frac{W_b}{g\varphi(\lambda')} + j \int_0^l m_w \, ds} \tag{24}$$

where

$$G = \frac{V_a \sin \tau \cos \tau}{j\dot{z}_o \cos \theta} = \frac{\kappa + 1 - j}{j}$$

The mass-correction factor j (eq. (9)) is plotted in figure 2 as a variation of j with trim angle. The approach parameter κ is defined as $\frac{\sin \tau}{\sin \gamma_o} \cos(\tau + \gamma_o)$ and is plotted in figure 3 as a function of trim angle and initial flight-path angle. Dividing equation (21) through by $\dot{z}_o^2$ and rearranging relates the vertical velocity, acceleration, and penetration as follows:

$$\frac{\ddot{z}}{\dot{z}_o^2} = - \frac{j^2 m_{w,s} \left(\frac{\dot{z}}{\dot{z}_o} + G \right)^2}{\frac{W_b \sin \tau}{g\varphi(\lambda')} + j \sin \tau \int_0^l m_w \, ds} \tag{25}$$

Equations (24) and (25) are the general equations of motion for any impact including the effects of carriage mass. These equations represent both bodies with the deeply immersed chine and the nonimmersed chine, depending only on the choice of the variables substituted. These equations are very similar to those derived in reference 2, the only difference being the inclusion of the mass correction factor j. When $j = 1$, equations (24) and (25) are identical to those of reference 2.

Immersed Chine

The general equations of motion, equations (24) and (25) may represent the deeply immersed chine if the proper substitutions are made. In this instance, let

$$Q_1 = \log_e \frac{\frac{\dot{z}}{\dot{z}_o} + G}{1 + G} + \frac{G}{\frac{\dot{z}}{\dot{z}_o} + G} - \frac{G}{1 + G}$$

Then equation (24) may be written as

$$Q_1 = - \int_0^z \frac{j \frac{m_{w,s}}{\sin \tau} \, dz}{\frac{W_b}{jg\varphi(\lambda')} + \int_0^l m_w \, ds} \tag{26}$$

Since from equation (12) it is assumed that $m_{w,s} = f(\zeta'_s)$, the integrals must be expressed in terms of ζ'_s. Therefore, the right-hand side of equation (26) is multiplied by $\frac{d\zeta'_s}{d\zeta'_s}$. Then, using the differential of

equation (18)$\left(d\zeta_s = \frac{dz}{\cos \tau}\right)$, as well as equation (14), and putting the result in nondimensional form by multiplying by $\rho b^3/\rho b^3$ yields the following equation:

$$Q_1 = -\int_0^{\zeta'_s/b} \frac{j \frac{m_{w,s}}{\rho b^2} \frac{d\zeta_s}{d\zeta'_s} d\frac{\zeta'_s}{b}}{\frac{C_\Delta \tan \tau}{j\varphi(\lambda')} + \int_0^{\zeta'_s/b} \frac{m_{w,s}}{\rho b^2} d\frac{\zeta'_s}{b}} \tag{27}$$

where $C_\Delta = \frac{W_b}{\rho g b^3}$.

Similarly, equation (25) can be written as

$$\frac{\ddot{z}b}{\dot{z}_o^2} = -\frac{j\left(\frac{\dot{z}}{\dot{z}_o} + G\right)^2 \frac{m_{w,s}}{\rho b^2 \cos \tau}}{\frac{C_\Delta \tan \tau}{j\varphi(\lambda')} + \int_0^{\zeta'_s/b} \frac{m_{w,s}}{\rho b^2} d\frac{\zeta'_s}{b}} \tag{28}$$

A time coefficient giving the relationship between displacement and time may also be defined as

$$t\frac{\dot{z}_o}{b} = \int_0^{z/b} \frac{d\frac{z}{b}}{\frac{\dot{z}}{\dot{z}_o}} \tag{29}$$

The following equations from reference 2 may be substituted into equations (27) and (28) for particular solutions:

For $\beta = 0^\circ$,

$$\frac{m_{w,s}}{\rho b^2} = \frac{\pi^3}{32} + 0.44 \frac{\zeta'_s}{b} \tag{30a}$$

For $\beta > 0^\circ$ and $\frac{\zeta'_s}{b} \leq \frac{\tan \beta}{2}$,

$$\frac{m_{w,s}}{\rho b^2} = \frac{\pi}{2}\left[\frac{\zeta'_s}{b} f(\beta)\right]^2 \tag{30b}$$

For $\beta > 0^\circ$ and $\frac{\zeta'_s}{b} > \frac{\tan \beta}{2}$,

$$\frac{m_{w,s}}{\rho b^2} = \frac{\pi}{8}\left[f(\beta)\tan \beta\right]^2 + \frac{B}{2}\left(\frac{\zeta'_s}{b} - \frac{\tan \beta}{2}\right) \tag{30c}$$

For equations (30), β is the angle of dead rise, $f(\beta)$ can be taken as $\frac{\pi}{2\beta} - 1$, and Bobyleff's flow coefficient B is obtained from figure 4 where it is plotted as a function of the angle of dead rise.

The aspect-ratio correction factor $\varphi(\lambda')$ can be obtained from figure 5, which gives the variation of $\varphi(\lambda')$ with λ'. The quantity λ' is found from the following equations (ref. 2):

For $\beta = 0^\circ$,

$$\lambda' = \frac{\zeta'_s}{b \tan \tau} \tag{31a}$$

For $\beta > 0^\circ$ and $\frac{\zeta'_s}{b} = \frac{\zeta_s}{b} \leqq \frac{\tan \beta}{2}$,

$$\lambda' = \frac{1}{\tan \tau\, f(\beta)} \tag{31b}$$

For $\beta > 0^\circ$ and $\frac{\zeta'_s}{b} = \frac{\zeta_s}{b} > \frac{\tan \beta}{2}$,

$$\lambda' = \frac{\left(\frac{\zeta'_s}{b}\right)^2}{\tan \tau\left(\frac{\zeta'_s}{b} - \frac{1}{4f(\beta)}\right)} \tag{31c}$$

The ratio $\frac{d\zeta_s}{d\zeta'_s}$ is found from figure 6 for angles of dead rise less than 10° and is taken as unity for larger angles of dead rise; the mass-correction factor j is obtained from figure 2.

Equations (27) and (28) may be simplified further by assuming that the acceleration of the virtual mass is negligible for the deeply immersed chine. Then equation (27) reduces to

$$Q_1 = \log_e \frac{\frac{\dot{z}}{\dot{z}_o} + G}{1 + G} + \frac{G}{\frac{\dot{z}}{\dot{z}_o} + G} - \frac{G}{1 + G}$$

$$= \int_0^{\zeta'_s/b} \frac{j^2 \varphi(\lambda') \frac{m_{w,s}}{\rho b^2} \frac{d\zeta_s}{d\zeta'_s} d\frac{\zeta'_s}{b}}{C_\Delta \tan \tau} \tag{32}$$

and equation (28) becomes

$$\frac{\ddot{z}b}{\dot{z}_o^2} = - \frac{j^2 \varphi(\lambda') \left(\frac{\dot{z}}{\dot{z}_o} + G\right)^2 \frac{m_{w,s}}{\rho b^2}}{C_\Delta \sin \tau} \tag{33}$$

A method utilizing figures 7 to 9 is presented in the appendix for solving equations (32) and (33). Note that the penetration parameter k_1 (fig. 8) and the three-dimensional mass parameter J_1 (fig. 9) are different from the parameters k and J of reference 2 because of the inclusion of the carriage-mass correction factor j, except when $j = 1$. The ratio of vertical penetration to beam may be easily found from the following relation (ref. 2):

$$\frac{z}{b} = \frac{\zeta'_s}{b} \frac{\zeta_s}{\zeta'_s} \cos \tau$$

$$= \lambda' \frac{\lambda}{\lambda'} \sin \tau \tag{34}$$

where λ/λ' may be obtained from figure 6 for angles of dead rise less than 10° and is taken as unity for larger angles of dead rise. This procedure is also demonstrated in the appendix for the maximum penetration.

Nonimmersed Chine

The equations of motion for the V-bottom float with nonimmersed chines can likewise be obtained from equations (24) and (25) to get the respective velocity and acceleration relationships. In this case, the effect of water rise at the keel is neglected. Furthermore, the function for the two-dimensional water mass can be written simply as

$$m_w = \left[f(\beta)\right]^2 \frac{\rho\pi}{2} \zeta^2 \tag{35}$$

where $f(\beta)$ is a constant depending on the dead rise of the float and is sometimes taken as $\frac{\pi}{2\beta} - 1$. (See refs. 1 and 2.)

Then, since $ds = d\zeta/\tan\tau$ and $\zeta_s = z/\cos\tau$,

$$\int_0^l m_w\, ds = \int_0^{\zeta_s} \left[f(\beta)\right]^2 \frac{\rho\pi}{2\tan\tau}\,\zeta^2\, d\zeta$$

$$= \frac{\rho\pi}{6\tan\tau}\left[f(\beta)\right]^2 \zeta_s^3 \tag{36}$$

Substituting equation (36) into (24) and simplifying yields the following result:

$$\frac{1}{j^2}\left(\log_e \frac{\frac{\dot{z}}{\dot{z}_o} + G}{1+G} + \frac{G}{\frac{\dot{z}}{\dot{z}_o} + G} - \frac{G}{1+G}\right) = -\int_0^{\zeta_s} \frac{\left[f(\beta)\right]^2 \frac{\rho\pi}{2}\,\zeta^2\, d\zeta}{\frac{W_b \tan\tau}{g\varphi(\lambda)} + \frac{j\rho\pi\left[f(\beta)\right]^2 \zeta^3}{6}} \tag{37}$$

After integration and rearrangement, equation (37) may be written

$$e^{\frac{G}{1+G} - \frac{G}{\frac{\dot{z}}{\dot{z}_o}+G}} = \frac{\frac{\dot{z}}{\dot{z}_o} + G}{1+G}\left[1 + \frac{gj\varphi(\lambda)\left[f(\beta)\right]^2 \rho\pi z^3}{6W_b \sin\tau\cos^2\tau}\right]^j$$

$$= \frac{\frac{\dot{z}}{\dot{z}_o} + G}{1+G}\left(1 + \frac{\alpha g j z^3}{W_b}\right)^j \tag{38}$$

where

$$\alpha = \frac{\rho\pi\varphi(\lambda)\left[f(\beta)\right]^2}{6\sin\tau\cos^2\tau}$$

Thus, equation (38) becomes

$$\left(1 + \frac{\alpha g j z^3}{W_b}\right)^j \frac{\frac{\dot{z}}{\dot{z}_o} + G}{1 + G} e^{\frac{G}{\frac{\dot{z}}{\dot{z}_o} + G} - \frac{G}{1+G}} - 1 = 0 \tag{39}$$

Similarly, equation (25) may be written

$$\frac{\ddot{z}}{\dot{z}_o^2} = - \frac{3\frac{\alpha g}{W_b} j^2 z^2 \left(\frac{\dot{z}}{\dot{z}_o} + G\right)^2}{1 + \frac{\alpha g j z^3}{W_b}} \tag{40}$$

Equations (39) and (40) are the equations of motion for the V-bottom float with nonimmersed chines. Equation (39) relates the velocity and penetration and equation (40) relates acceleration, velocity, and penetration.

When equations (39) and (40) are put in a generalized form similar to that of reference 1, the following expressions result:

(a) Generalized displacement

$$u = \left(\frac{\alpha g}{W_b}\right)^{1/3} z$$

$$= \left(\frac{1}{j} \left\{ \left[\frac{1 + G}{\frac{\dot{z}}{\dot{z}_o} + G} e^{G\left(\frac{1}{1+G} - \frac{1}{\frac{\dot{z}}{\dot{z}_o} + G}\right)} \right]^{1/j} \right\} - 1 \right)^{1/3} \tag{41}$$

(b) Generalized acceleration

$$u'' = \left(\frac{W_b}{\alpha g}\right)^{1/3} \frac{\ddot{z}}{\dot{z}_o^2}$$

$$= 3j^{4/3}\left(\frac{\dot{z}}{\dot{z}_o} + G\right)^2 \left(\left[\frac{\frac{\dot{z}}{\dot{z}_o} + G}{1 + G} e^{G\left(\frac{1}{\frac{\dot{z}}{\dot{z}_o} + G} - \frac{1}{1+G}\right)} \right]^{1/j} \left\{ 1 - \left[\frac{\frac{\dot{z}}{\dot{z}_o} + G}{1 + G} e^{G\left(\frac{1}{\frac{\dot{z}}{\dot{z}_o} + G} - \frac{1}{1+G}\right)} \right]^{1/j} \right\}^2 \right)^{1/3} \tag{42}$$

$$u'' = \frac{3j^2u^2\left(\frac{\dot{z}}{\dot{z}_o} + G\right)^2}{1 + ju^3} \tag{43}$$

(c) Generalized time

$$\sigma = \int_0^u \frac{\dot{z}_o}{\dot{z}}\,du = \int_1^{\dot{z}/\dot{z}_o} \frac{1}{u''}\,d\frac{\dot{z}}{\dot{z}_o} \tag{44}$$

(d) Generalized pitching moment

$$m = \frac{M}{\dot{z}_o^2}\frac{\varphi(\lambda)}{\varphi_1(\lambda)}\frac{\sin\tau\cos\tau}{\frac{W_b}{g}}$$

$$= \frac{\left[f(\beta)\right]^2\rho\pi\varphi(\lambda)g}{6\sin\tau\cos^2\tau W_b}\left[\frac{j\ddot{z}z^4}{4\dot{z}_o^2} + \left(j\frac{\dot{z}}{\dot{z}_o} + jG\right)^2 z^3\right]$$

$$= \frac{uu''}{3}\left(1 + \frac{ju^3}{4}\right) \tag{45}$$

where $\varphi_1(\lambda)$ is the pitching-moment aspect-ratio correction and is sometimes taken as $\varphi(\lambda)$. (See ref. 1.)

(e) Generalized center-of-pressure distance

$$p = \frac{m}{u''} = \frac{u}{3}\left(1 + \frac{ju^3}{4}\right) \tag{46}$$

RESULTS AND DISCUSSION

The general equations of motion (eqs. (24) and (25)) are applicable to any prismatic body. However, because of the nature of the general equations, the determination of the carriage-mass effect for the completely general case cannot be shown; thus the analysis is limited to more specific cases. For this reason, two examples - the deeply immersed chine and the nonimmersed chine - are treated separately. For the immersed

chine the flat plate is selected as the configuration, whereas for the nonimmersed chine the V-bottom float is given a generalized treatment.

The general approach is to plot some of the important parameters with carriage mass varied in order to show its effect. For simplicity, the two end conditions are chosen, namely, the condition for zero carriage mass and the condition for an infinite carriage mass. The difference between these two conditions represents the maximum effect of a carriage mass.

Figure 2 shows the variation of the mass correction factor j with the trim for various ratios of carriage mass to float mass. These curves indicate trim angles and mass ratios that approach the conditions for zero or infinite carriage mass. The carriage-mass effect upon the correction factor is more important at high trims and the mass ratios of magnitude 10 are found to approach that of the infinite carriage mass. At the low trims the effect of a carriage mass is small since the mass correction factor approaches 1.0, the free-body case.

Nonimmersed Chine

The nonimmersed chine is discussed first because a more general solution is possible in this case, and it is believed that maximum percentage corrections for the various parameters due to a carriage mass which apply to the nonimmersed chine can also be applied to the immersed chine as a first approximation.

For the V-bottom float with the nonimmersed chine the equations of motion are put in the generalized form of reference 1. The generalized coefficients given by equations (41) to (46) are then plotted in figure 10 for zero and infinite carriage masses at maximum acceleration and maximum penetration to give some indication of carriage-mass effect. The vertical-velocity ratio is given a similar treatment and is plotted at maximum acceleration and rebound. (See fig. 10(b).) The curves for the zero carriage mass are taken from reference 1.

The curves indicate that the maximum carriage-mass effect varies with the trim and the approach parameter. At low trims there is little carriage effect, inasmuch as the carriage mass imposes inertia only in the horizontal direction and at low trims there is little water reaction in this direction. At high trims and low approach parameters (high flight-path angles), all the coefficients are affected by carriage mass; whereas for high trims and high approach parameters (low flight-path angles), only the vertical-velocity ratio, acceleration, and pitching-moment coefficients are noticeably affected.

Figure 3 shows that at the low approach parameters ($\kappa < 1$) and high trims ($\tau \geq 15^{\circ}$) the flight-path angles are larger than those usually

expected with the modern seaplane. However, in certain instances, such as impacts subsequent to the initial seaplane impact, very high flight-path angles may occur. Also, although the low range of approach parameter may be out of the normal operating range of the seaplane, it still has significance as far as testing programs are concerned. This situation exists since testing programs are conducted over an entire range of variables if possible; therefore tests including the low range of approach parameters could lead to erroneous conclusions if the carriage-mass effect is not considered. Finally, some new or unusual configurations such as certain types of hydro-skis may be normally operated in the low range of approach parameters.

It is also deemed important to give an idea of carriage-mass effect in the more usual ranges of flight paths and trims. At trims up to and including 15° and approach parameters larger than unity, there is about 10 percent or less correction to any of the coefficients plotted. (See fig. 10.) More specifically, at a trim of 15° and a flight-path angle of 5.5° ($\kappa = 2.4$) the maximum percentage changes in some of the generalized coefficients are as follows: -1.5 in maximum displacement, 2 in displacement at maximum acceleration, -8 in velocity at maximum acceleration, -6 in velocity at rebound, 2 in maximum acceleration, 6 in acceleration at maximum penetration, 4 in pitching-moment at maximum penetration, and 2.5 in pitching-moment at maximum acceleration. The changes in center of pressure and time are small at either maximum acceleration or maximum penetration. This specific case shows that some of the variables are changed much less than the 10 percent maximum quoted previously.

From figure 10 it is possible to observe how a carriage mass influences the various parameters during an impact. The maximum penetration and time to reach maximum penetration are decreased, and the acceleration at maximum penetration is increased. The maximum acceleration, time to reach maximum acceleration, and displacement at maximum acceleration are increased, but the vertical velocity at maximum acceleration is decreased. Carriage effect also decreases the rebound velocity (increases in the negative direction, fig. 10(b)) which has an important effect on subsequent impacts. The pitching moment is increased at both maximum acceleration and maximum penetration, whereas the center-of-pressure distance is increased at maximum acceleration and decreased at maximum penetration.

Immersed Chine

For the immersed chine, the exact solution for the equations of motion are laborious, and as a simplification the acceleration of the virtual mass is considered negligible. According to reference 2, this simplification does not seriously reduce the accuracy of the solutions for practical landing configurations if the beam loading is greater than 1.0 and the chines are appreciably immersed. Under the foregoing

assumption, the equations of motion (eqs. (24) and (25)) reduce to equations (32) and (33). A method by which equations (32) and (33) can be solved is presented in the appendix.

As an example for the immersed chine, a flat plate is assumed as the impacting body and the equations of motion are solved by use of the method presented in the appendix for both the infinite carriage mass and the zero carriage mass. The solution is made at maximum penetration and maximum acceleration and curves are presented at these conditions.

Figure 11 shows the variation of the maximum penetration with various initial conditions for both zero and infinite carriage masses. Figure 12 shows the variation of the maximum impact lift coefficient against the same parameters. These curves indicate, like those for the V-bottom float with nonimmersed chines, that the mass effect is more pronounced at high trims and high flight-path angles (low approach parameters). In addition, figure 11 shows a slight effect of maximum penetration with beam at a flight-path angle of 5.5°. However, this effect is not noted in general and may be due to computational or procedural errors.

For the flat plate with immersed chines and the V-bottom float with nonimmersed chines, the maximum percentage change in maximum penetration and maximum acceleration due to a carriage mass are of the same order for comparable trim and flight-path conditions. This comparison was made for trims of 15°, 30°, and 45° and flight-path angles of 2.5°, 5.5°, 10° and 20°. For instance, the maximum change in maximum penetration at a flight-path angle of 20° and trims of 15°, 30°, and 45° is about -5, -9, and -14 percent, respectively, for the nonimmersed chine and is about -4, -7, and -13 percent for the immersed chine. The maximum change in maximum acceleration is about 2, 9, and 21 percent for the nonimmersed chine and about 2, 9, and 23 percent for the immersed chine. The percentage corrections for the immersed chine are averaged over the beam-loading range, although there was little variation throughout the range from 1 to 100.

From calculations of vertical-velocity ratio for the immersed chine the same conclusion was arrived at for the velocity at maximum acceleration, namely, that the maximum percentage correction due to carriage effect was about the same for the flat plate with immersed chines and the V-bottom float with nonimmersed chines. It might be expected that for the other variables the maximum percentage corrections at maximum acceleration and maximum penetration is of the same order also, although this has not been proved.

CONCLUDING REMARKS

A method has been derived for theoretically including the effect of a carriage mass in the equations of motion for any impacting prismatic body. The equations are solved for the V-bottom float with nonimmersed chines and the flat plate with deeply immersed chines. The maximum effect of carriage mass upon the loads and motions of the nonimmersed chine at maximum penetration and maximum acceleration varies with trim and flight-path angle. At low trims the effect of a carriage mass is small. At high flight-path angles and high trims (low approach parameter), carriage mass has an effect on all the variables plotted; whereas at high trims and low flight-path angles (high approach parameter), carriage mass has an effect upon the velocity ratio, acceleration, and pitching moment only.

For the more usual seaplane-design conditions, that is, approach parameters larger than 1.0 and trims up to 15°, the maximum percentage correction for any of the coefficients at the conditions presented is about 10 percent or less.

For the V-bottom float with nonimmersed chines at the condition of maximum penetration, a carriage mass tends to decrease maximum displacement, time to reach maximum penetration, and center-of-pressure distance, whereas it tends to increase the acceleration and pitching moment. At maximum acceleration, carriage mass increases the displacement, acceleration, time to reach maximum acceleration, pitching moment, and center-of-pressure distance, whereas it decreases the vertical velocity. The vertical velocity at rebound is also decreased (increased in the negative direction).

The maximum percentage change in maximum penetration and maximum acceleration due to carriage effect is of the same order for both the V-bottom float with nonimmersed chines and the flat plate with deeply immersed chines at flight-path angles of 2.5°, 5.5°, 10°, and 20° and trims of 15°, 30°, and 45° for beam loadings from 1 to 100.

Langley Aeronautical Laboratory,
National Advisory Committee for Aeronautics,
Langley Field, Va., November 17, 1955.

APPENDIX

COMPUTATIONAL PROCEDURES

The simplified methods for computing some impact parameters for the deeply immersed chines are presented. These methods, including effect of carriage mass, are based on a solution of the equations of motion (eqs. (32) and (33)), which have the following restrictions: the acceleration of the virtual mass, the effect of flight-path angle on water rise at the keel, and the effect of flight-path angle on the rate of change of water rise at the keel are neglected. The result of these omissions is considered small at beam loadings larger than unity. Applicability is also restricted to impacts for which the leading edge of the surface is not immersed. The procedures are similar to the method presented in reference 2, appendix B, procedure 1.

Procedure I

The steps for obtaining maximum penetration z/b_{max} are as follows:

(1) Set $\frac{\dot{z}}{\dot{z}_o} = 0$.

(2) Obtain $G = \frac{\kappa + 1 - j}{j}$, where κ can be obtained from figure 3 and j from figure 2.

(3) Use G and $\dot{z}/\dot{z}_o$ to obtain Q_1 from figure 7.

(4) With Q_1, C_Δ, and τ, calculate $k_1 = -\frac{C_\Delta Q_1}{j^2}$, where $C_\Delta = \frac{W_b}{\rho g b^3}$.

(5) With k_1, τ, and β, obtain ζ'_s/b from figure 8.

(6) From

$$\frac{z}{b} = \frac{\zeta'_s}{b}\frac{\zeta_s}{\zeta'_s}\cos\tau$$

$$= \lambda'\frac{\lambda}{\lambda'}\sin\tau$$

obtain z/b_{max} where λ/λ' is taken from figure 6 for $\beta < 10^{\circ}$. For larger values of β, the ratio λ/λ' is taken as unity.

Procedure II

The impact lift coefficient at maximum load $C_{L_{max}}$ may be computed in the following manner:

(1) Compute value of $G = \frac{\kappa + 1 - j}{j}$, where κ can be obtained from figure 3 and j from figure 2.

(2) Select several values of vertical-velocity ratio $\dot{z}/\dot{z}_o$ between 1 and -1 and, with the value of G, obtain a value of Q_1 from figure 7 for each value of $\dot{z}/\dot{z}_o$.

(3) Compute a value of k_1 for each value of Q_1 from the equation $k_1 = \frac{C_\Delta Q_1}{j^2}$, where $C_\Delta = \frac{W_b}{\rho g b^3}$.

(4) Obtain values of the ratio of normal penetration to beam ζ'_s/b for each value of k_1 from figure 8 with use of appropriate values of τ and β.

(5) Obtain value of J_1 from figure 9 for each value of ζ'_s/b by use of appropriate values of τ and β.

(6) Calculate the value of the acceleration ratio $\ddot{z}b/\dot{z}_o^2$ for each value of $\dot{z}/\dot{z}_o$ and $\zeta'_s b$ through substitution into

$$\frac{\ddot{z}b}{\dot{z}_o^2} = -j^2\left(\frac{\dot{z}}{\dot{z}_o} + G\right)^2 \frac{J_1}{C_\Delta}$$

(7) Find the values at which $zb\,\dot{z}_o^2$ is maximum, and then compute

$$C_L = 2 \sin^2\gamma_o j^2\left(\frac{\dot{z}}{\dot{z}_o} + G\right)J_1$$

Additional Procedures

Variations of procedures I and II may be used to give additional information. For instance, if the vertical-velocity ratio $\dot{z}/\dot{z}_o$ is set equal to zero and the steps of procedure II are followed, the load at maximum penetration can be found. The penetration at maximum load can be obtained by utilization of the ratio ζ'_s/b at maximum load in conjunction with equation (34) which is presented in step (6), procedure I. In order to obtain the variation of time with penetration equation (29). must be either graphically or numerically integrated.

REFERENCES

1. Milwitzky, Benjamin: Generalized Theory for Seaplane Impact. NACA Rep. 1103, 1952.

2. Schnitzer, Emanuel: Theory and Procedure for Determining Loads and Motions in Chine-Immersed Hydrodynamic Impacts of Prismatic Bodies. NACA Rep. 1152, 1953. (Supersedes NACA TN 2813.)

3. Mayo, Wilbur L.: Analysis and Modification of Theory for Impact of Seaplanes on Water. NACA Rep. 810, 1945. (Supersedes NACA TN 1008.)

4. Smiley, Robert F.: The Application of Planing Characteristics to the Calculation of the Water-Landing Loads and Motions of Seaplanes of Arbitrary Constant Cross Section. NACA TN 2814, 1952.

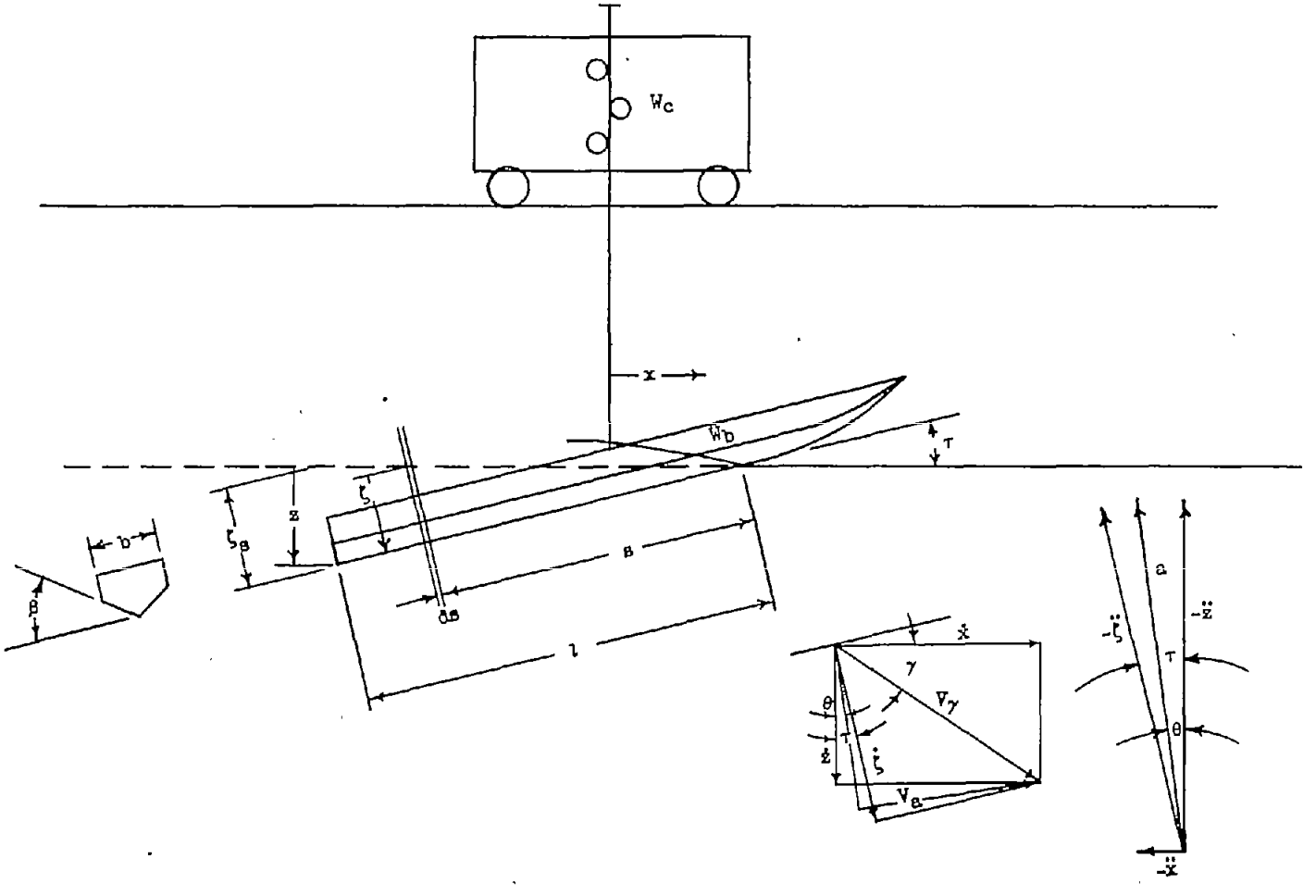

(a) Body with dead rise.

Figure 1.- Geometric relations during impact.

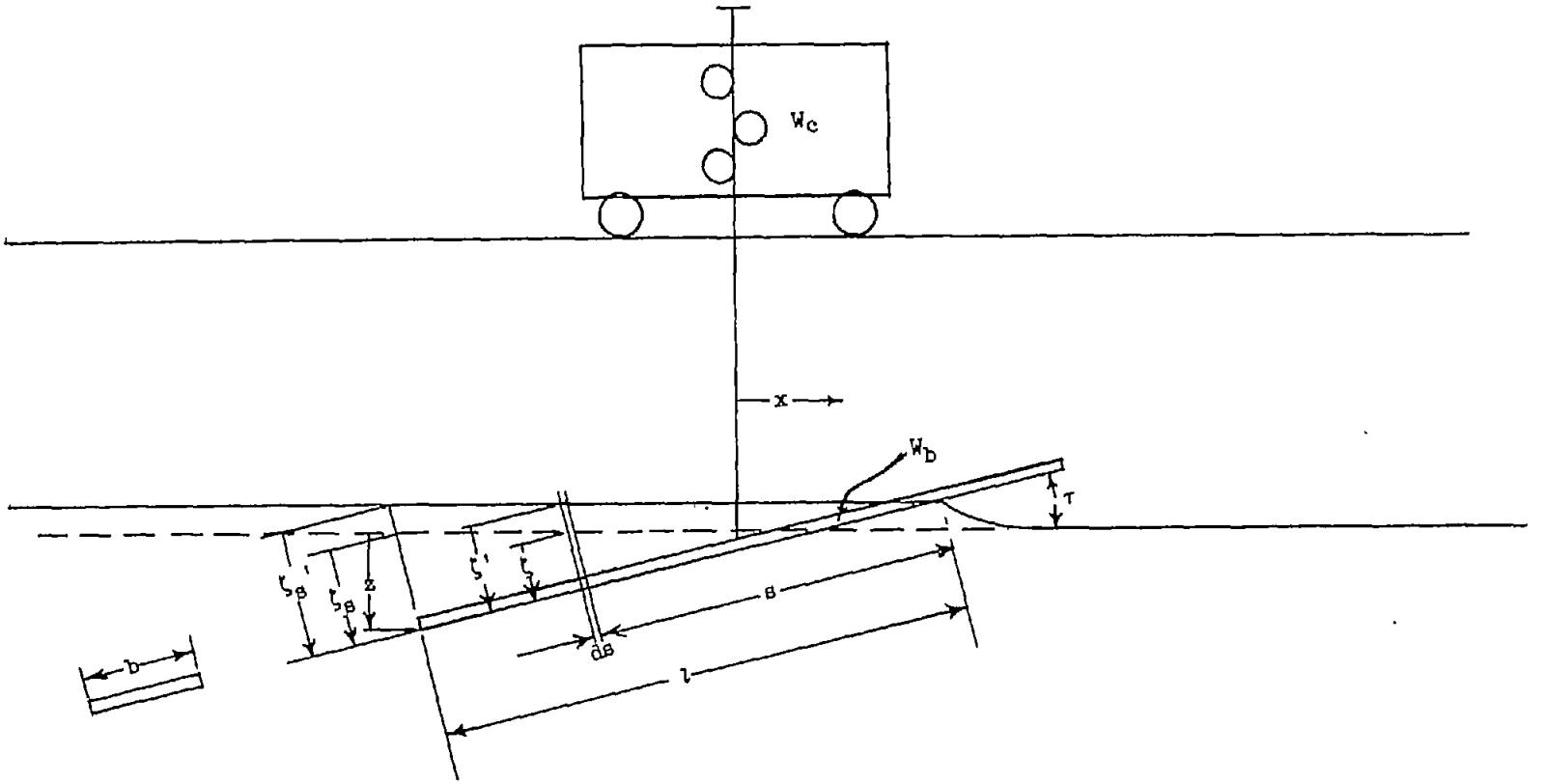

(b) Flat plate.

Figure 1.- Concluded.

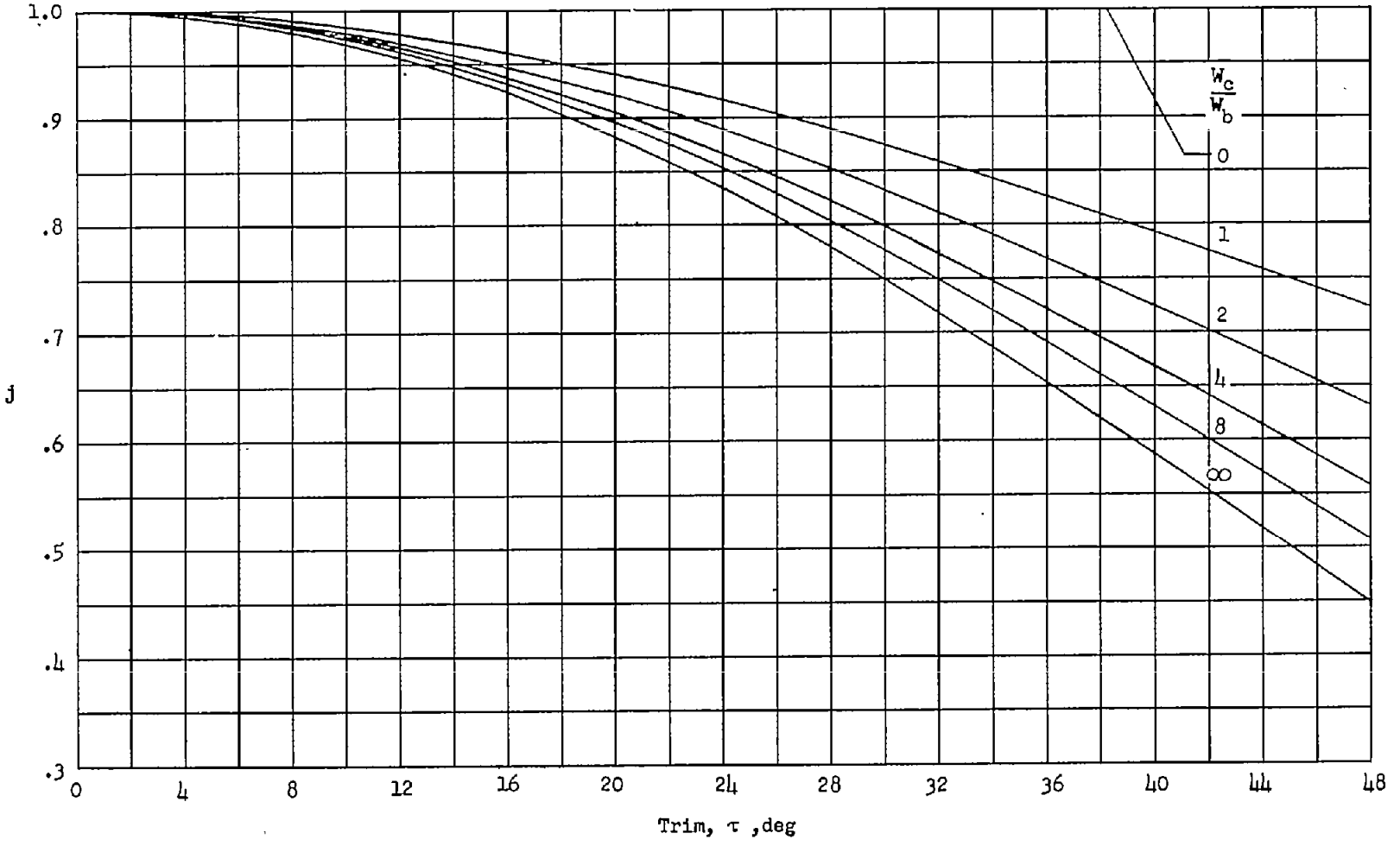

Figure 2.- Variation of carriage-mass correction factor with trim and mass ratio.

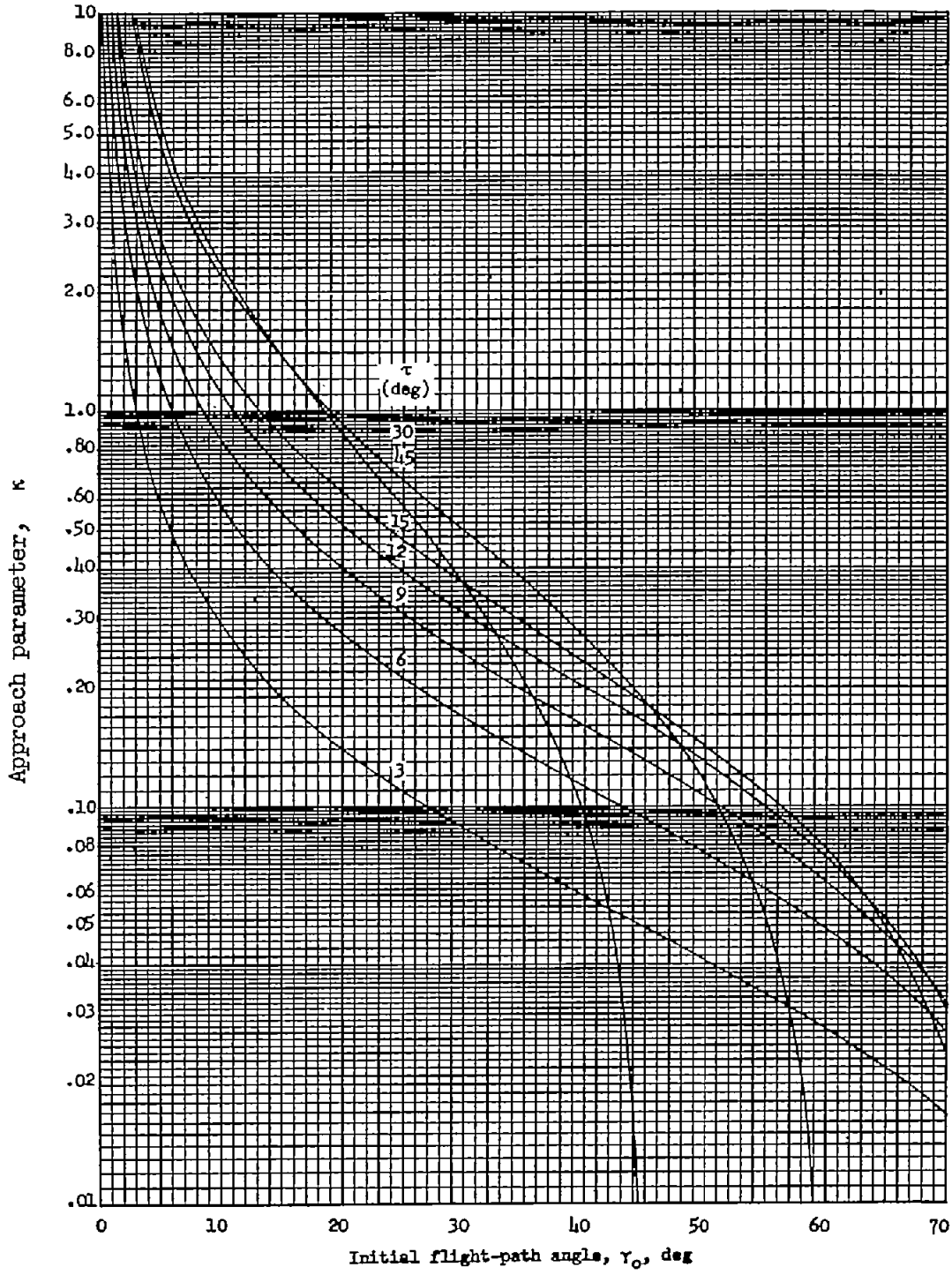

Figure 3.- Variation of approach parameter with trim and flight-path angle.

$$\kappa = \frac{\sin \tau}{\sin \gamma_0} \cos (\tau + \gamma_0).$$

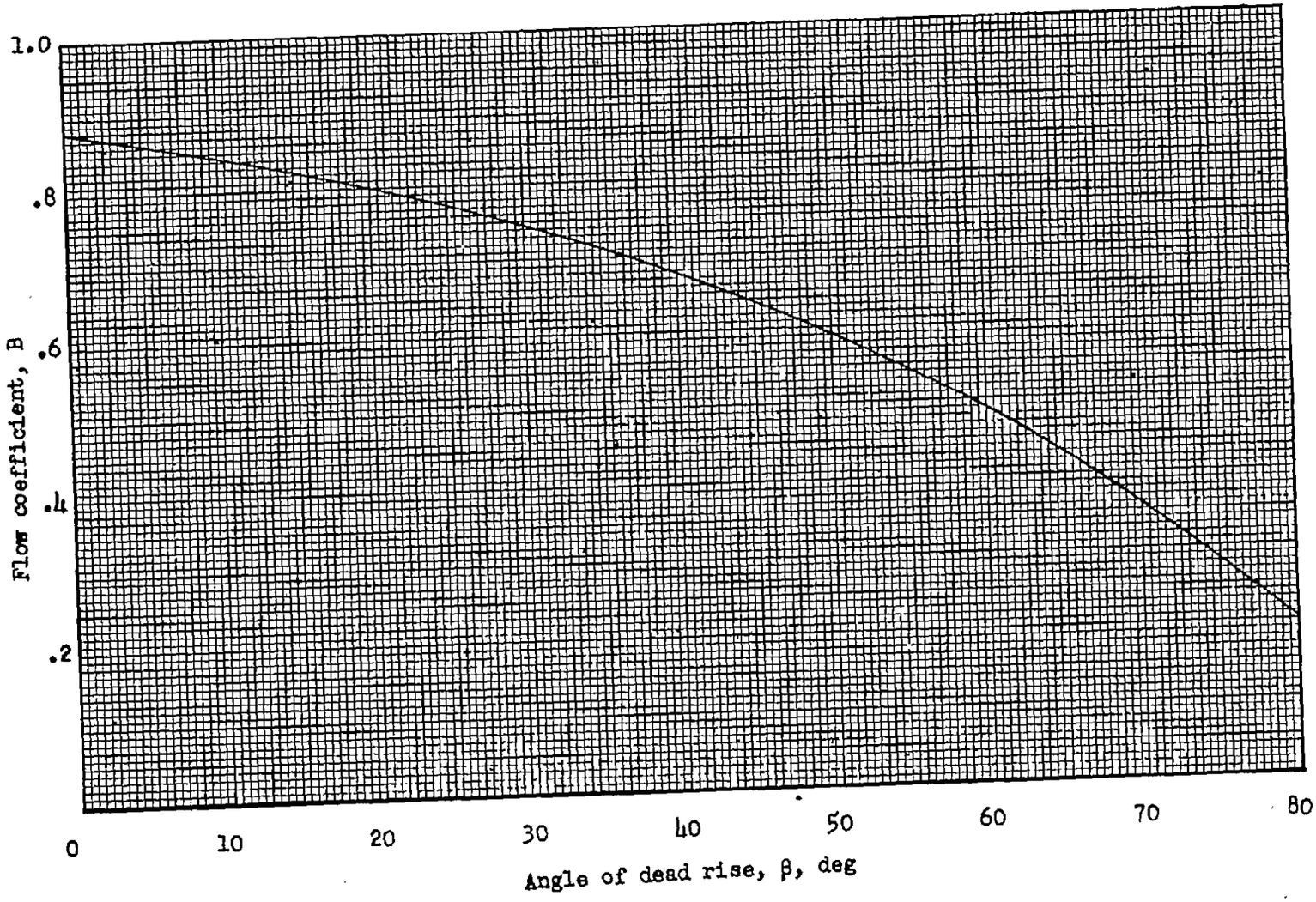

Figure 4.- Variation of flow coefficient with angle of dead rise (ref. 2).

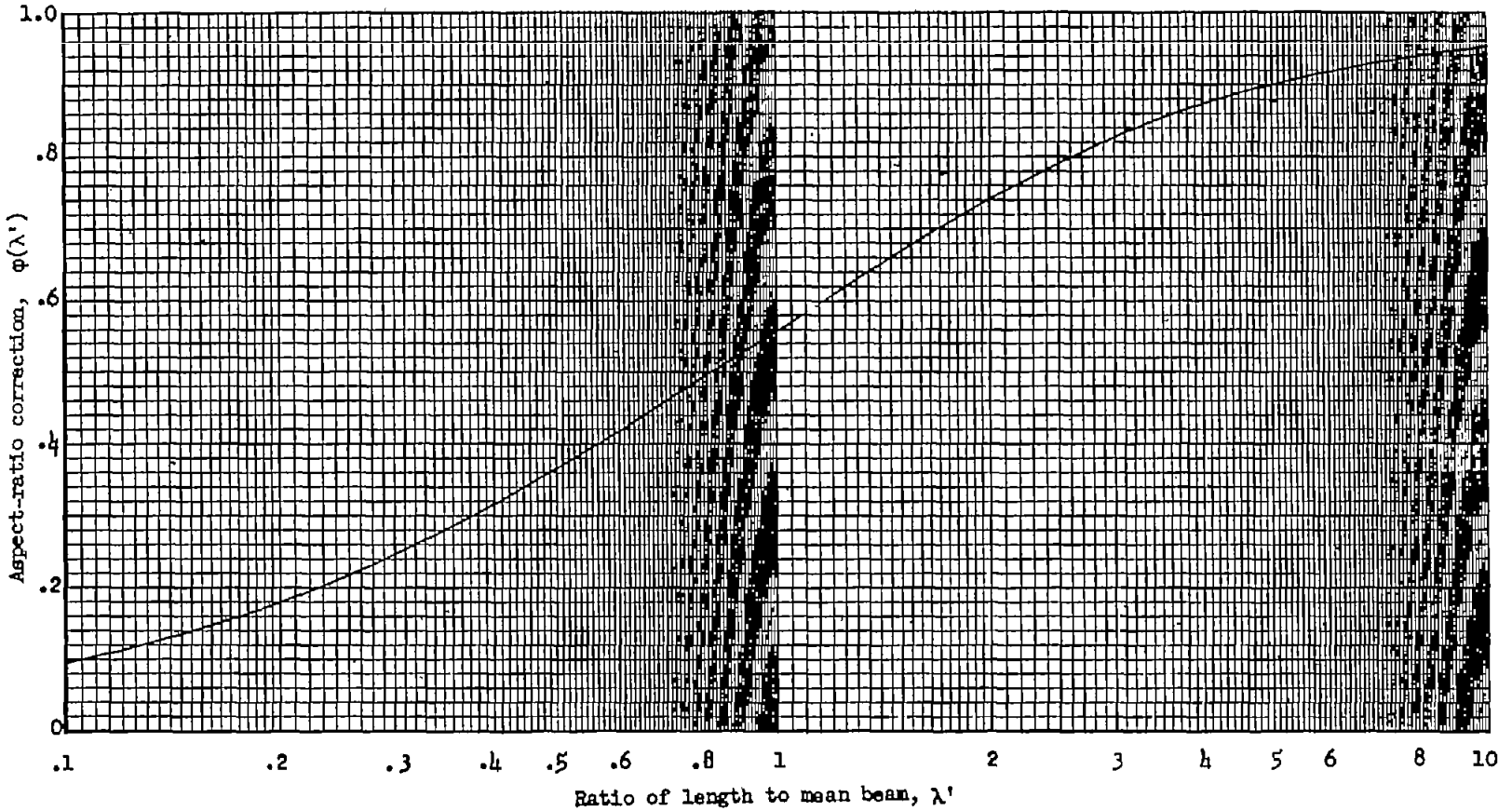

Figure 5.- Pabst's aspect-ratio correction factor for three-dimensional flow (ref. 2). $\varphi(\lambda') = \left[\frac{1}{1 + \frac{1}{(\lambda')^2}}\right]^{1/2}\left(1 - \frac{0.425}{\lambda' + \frac{1}{\lambda'}}\right)$.

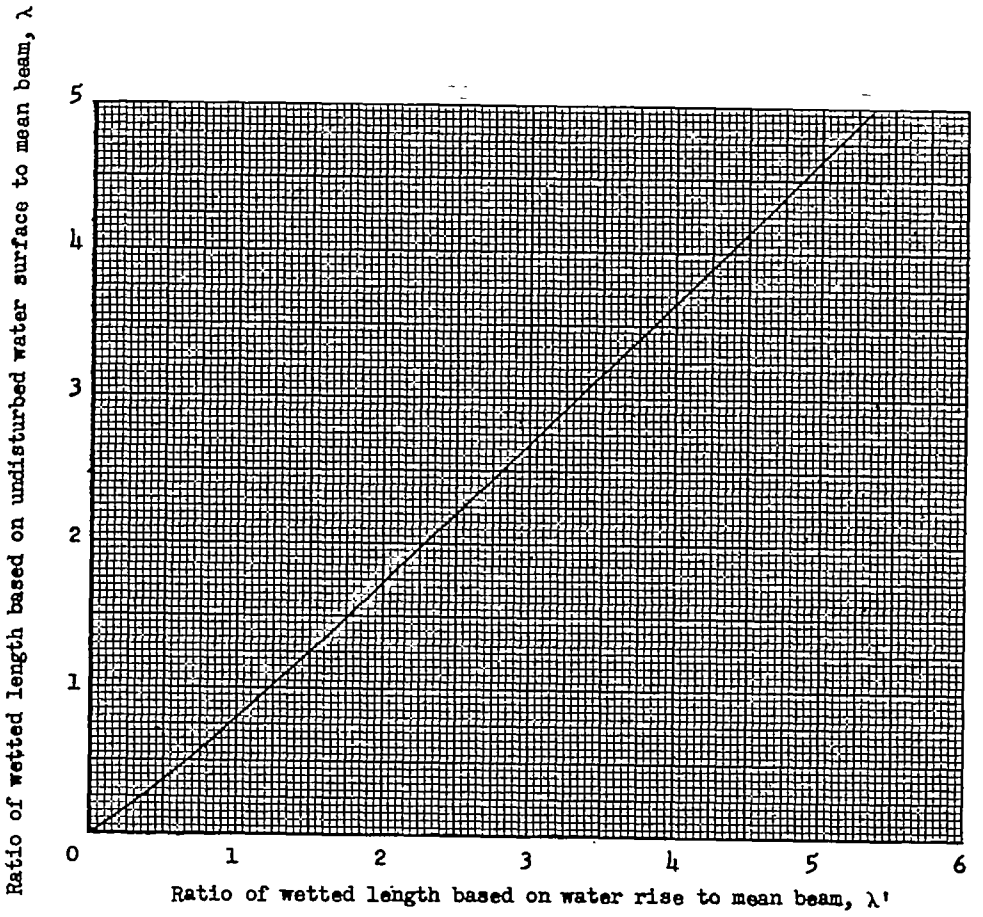

(a) Wetted-length variations.

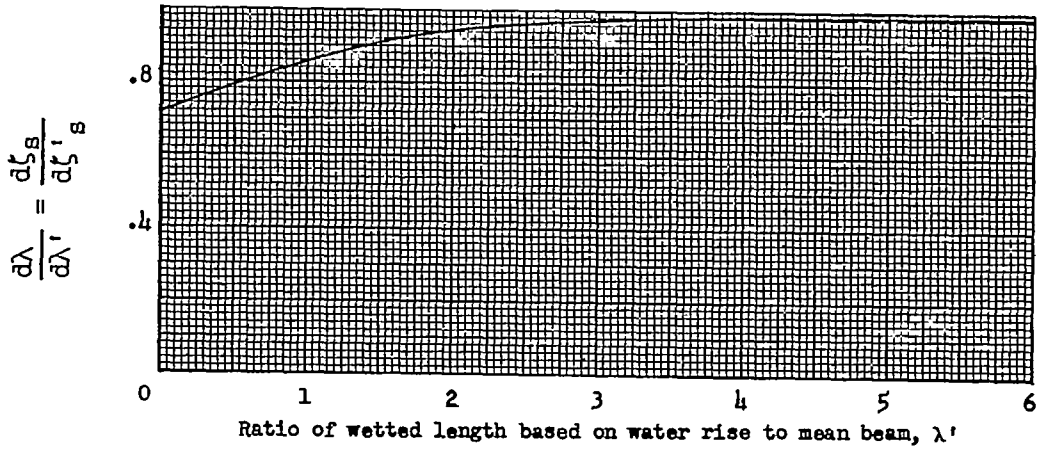

(b) Variation of derivative of wetted-length ratio with ratio of wetted length based on water rise to mean beam.

Figure 6.- Water-rise variations for a flat plate (ref. 2).

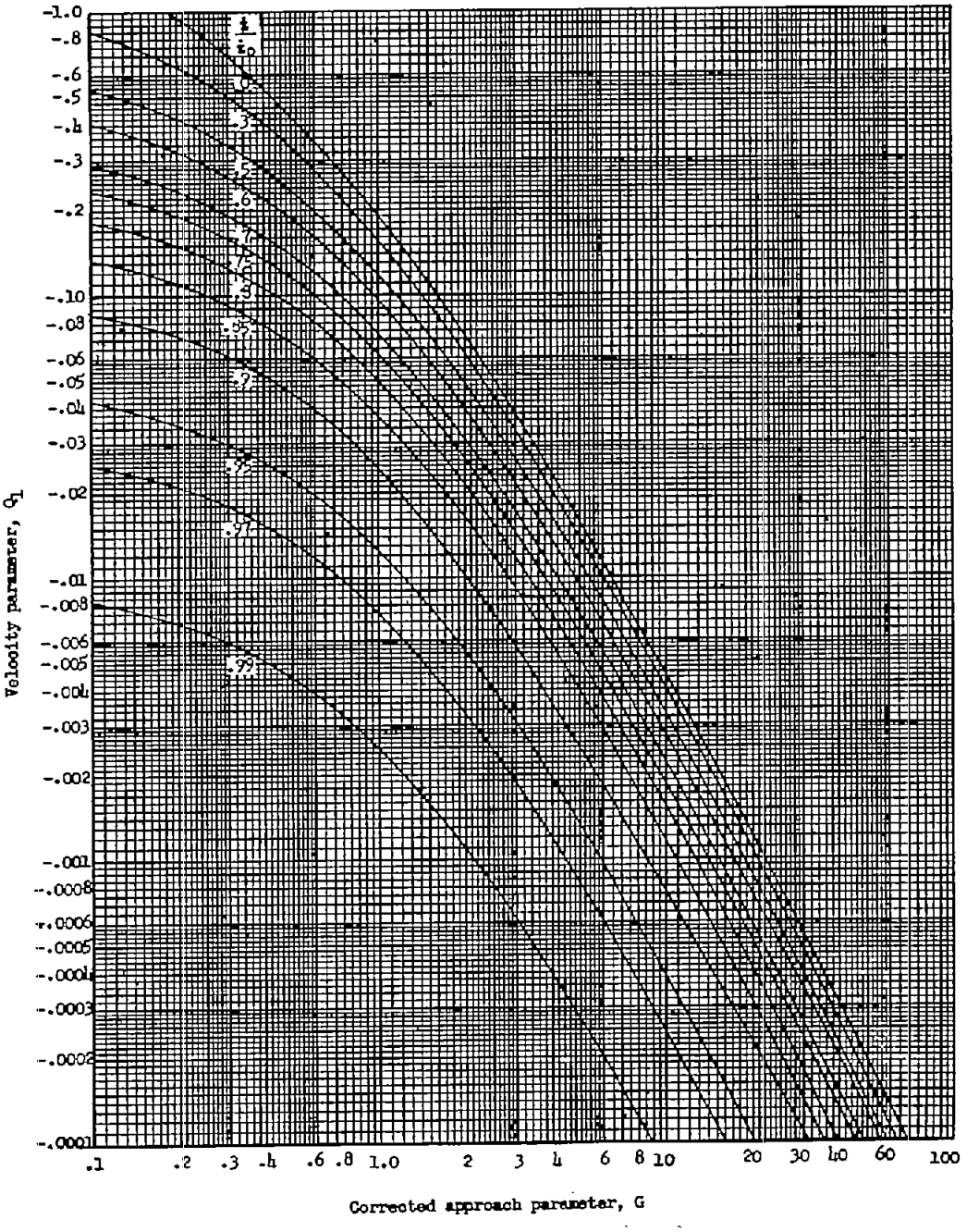

(a) Penetration.

Figure 7.- Variation of velocity parameter with corrected approach parameter for various velocity ratios (ref. 2).

$$Q = \log_e \frac{\frac{\dot{z}}{\dot{z}_o} + G}{1 + G} + \frac{G}{\frac{\dot{z}}{\dot{z}_o} + G} - \frac{G}{1 + G}.$$

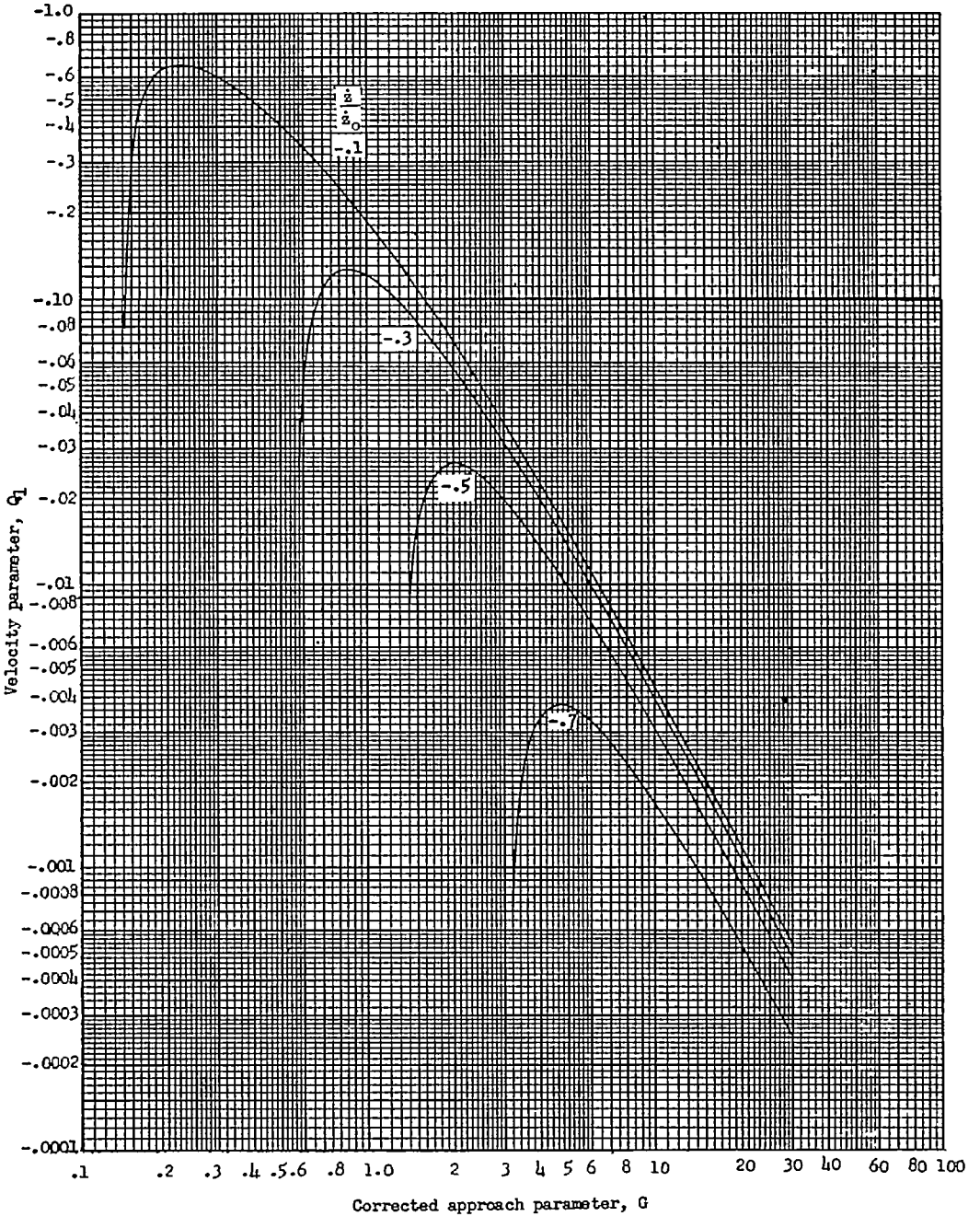

(b) Rebound.

Figure 7.- Concluded.

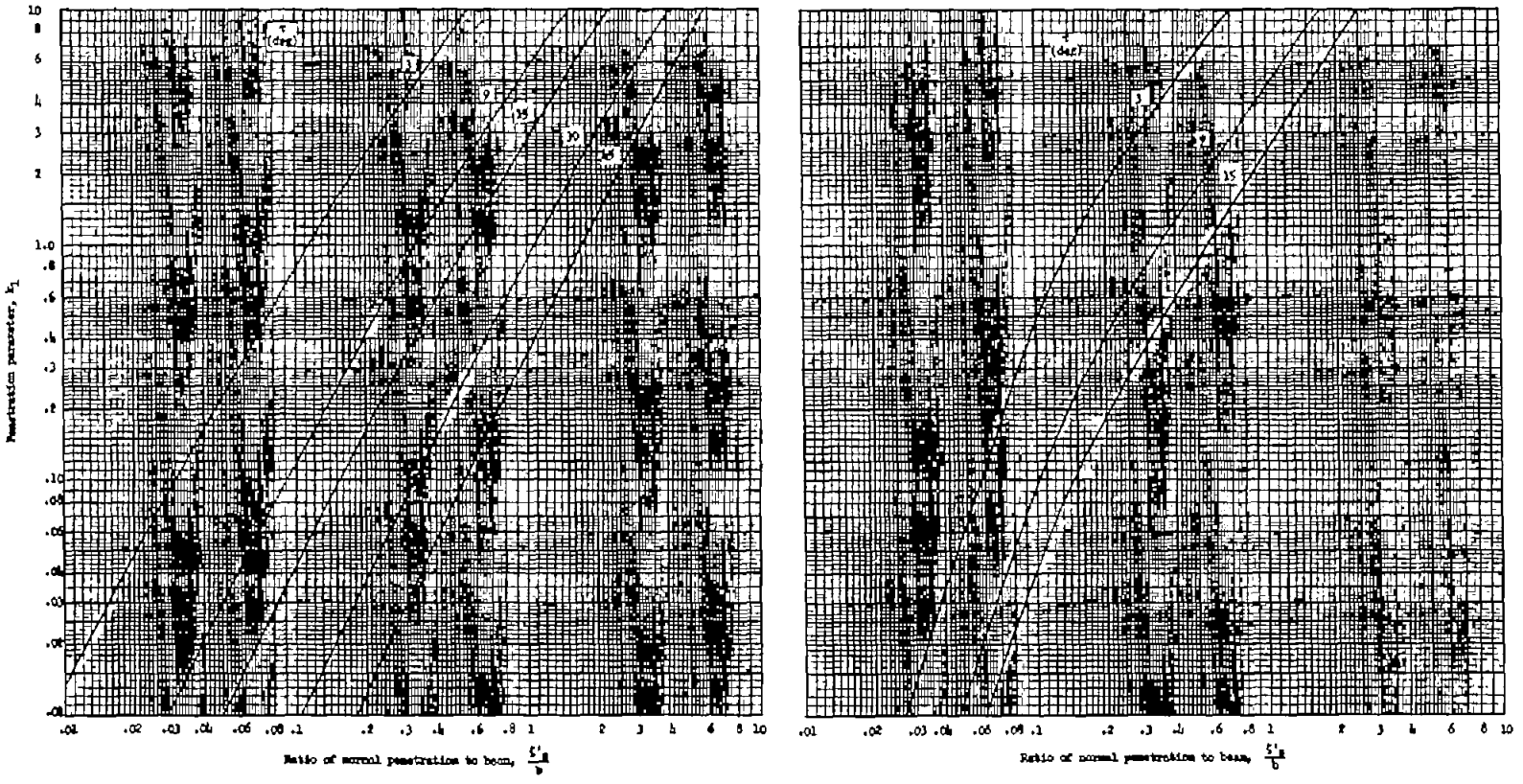

(a) $\beta = 0^{\circ}$.

(b) $\beta = 10^{\circ}$.

Figure 8.- Variation of penetration parameter for various angles of dead rise (ref. 2).

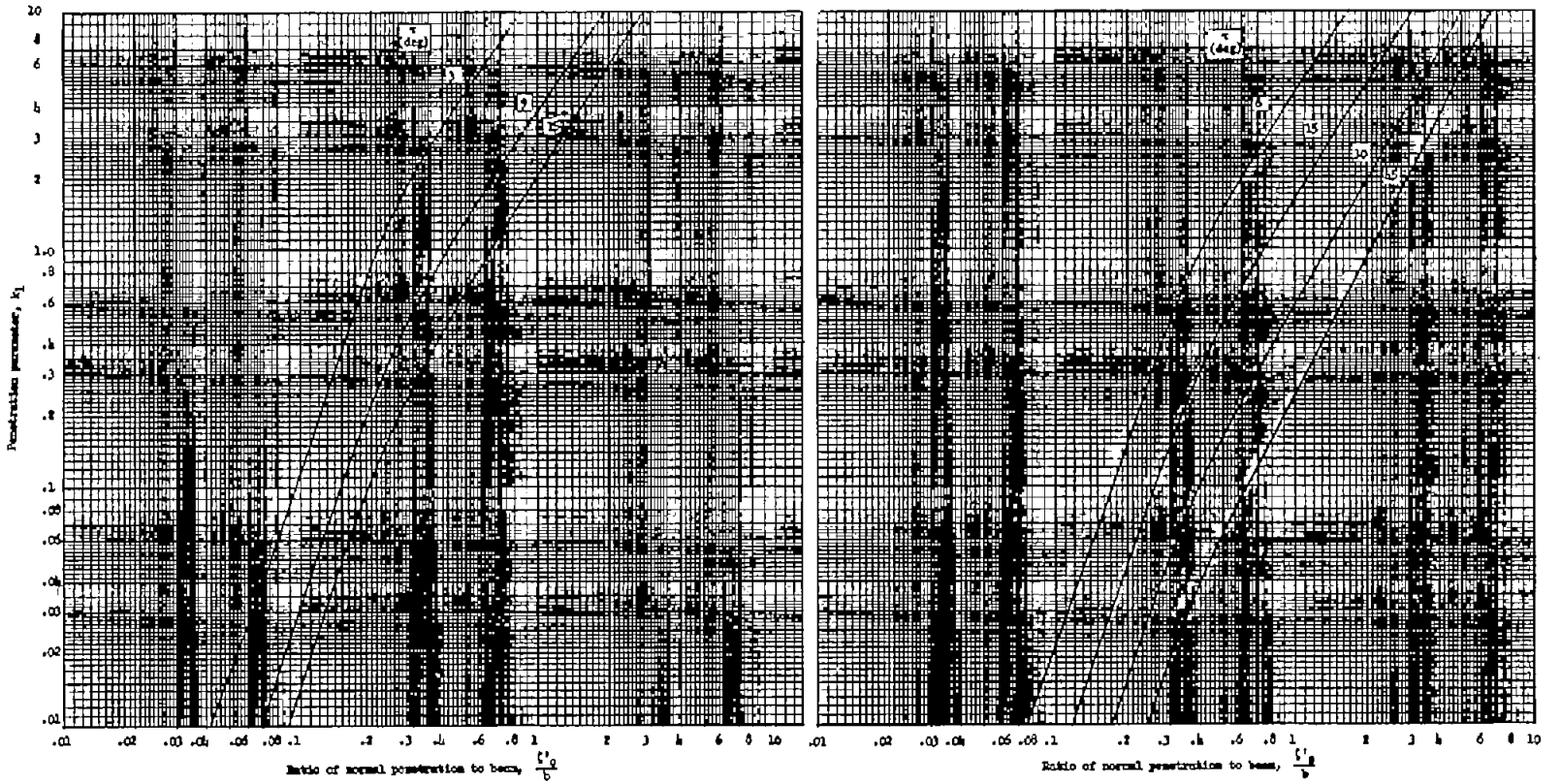

(c) $\beta = 20^\circ$.

(d) $\beta = 30^\circ$.

Figure 8.- Concluded.

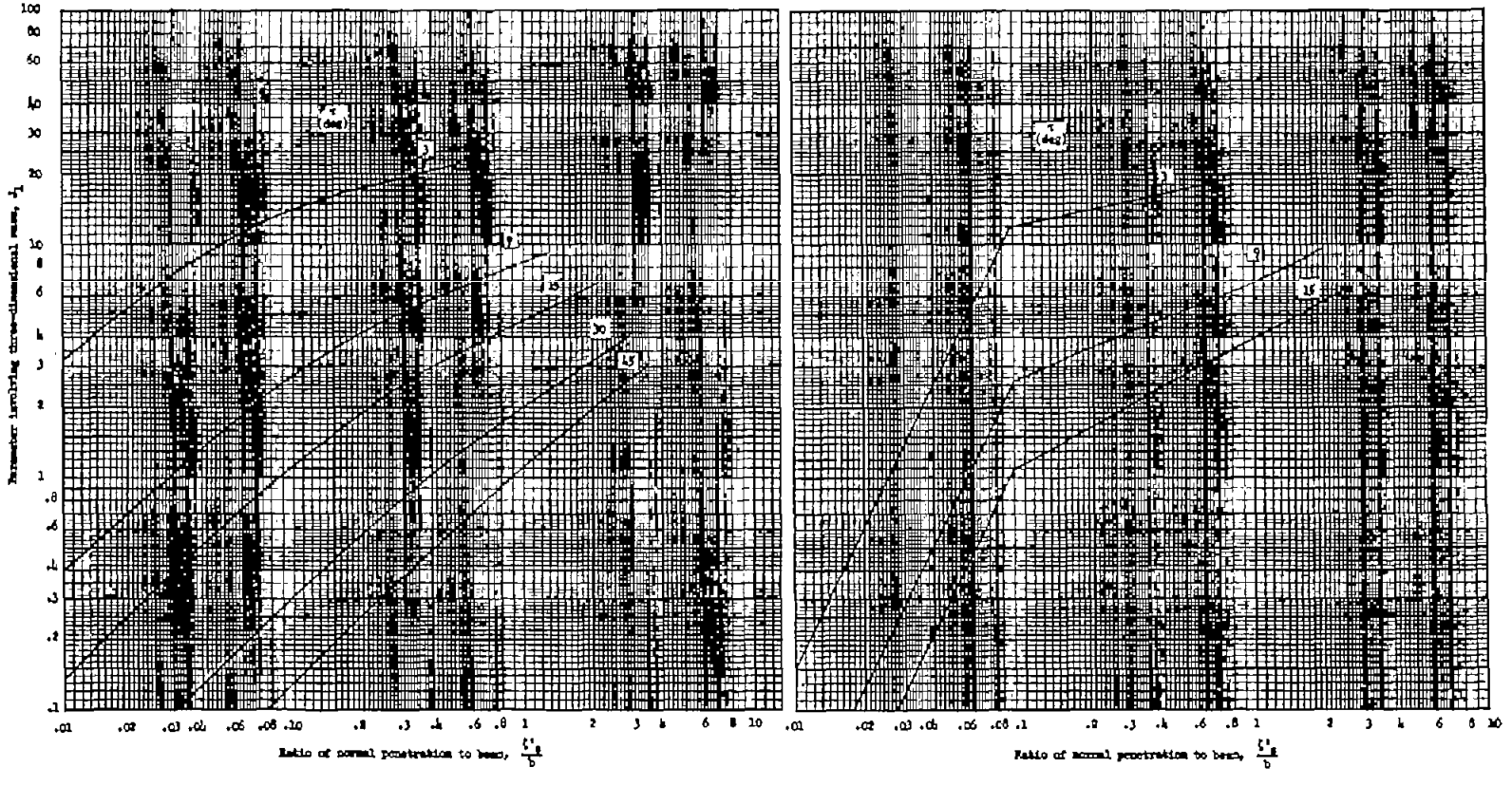

(a) $\beta = 0^\circ$.

(b) $\beta = 10^\circ$.

Figure 9.- Variation of parameter involving three-dimensional mass for various angles of dead rise (ref. 2).

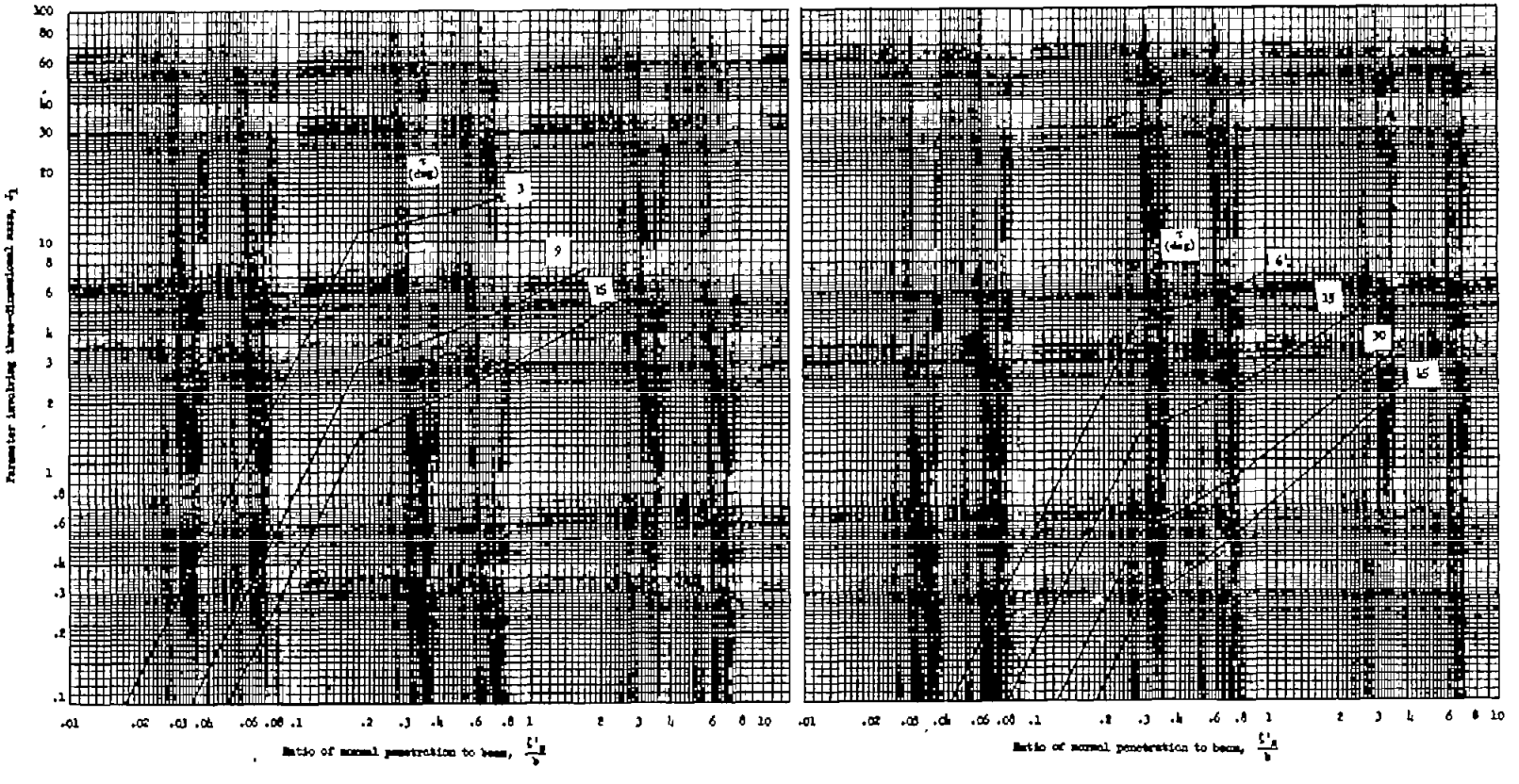

(c) $\beta = 20^\circ$.

(d) $\beta = 30^\circ$.

Figure 9.- Concluded.

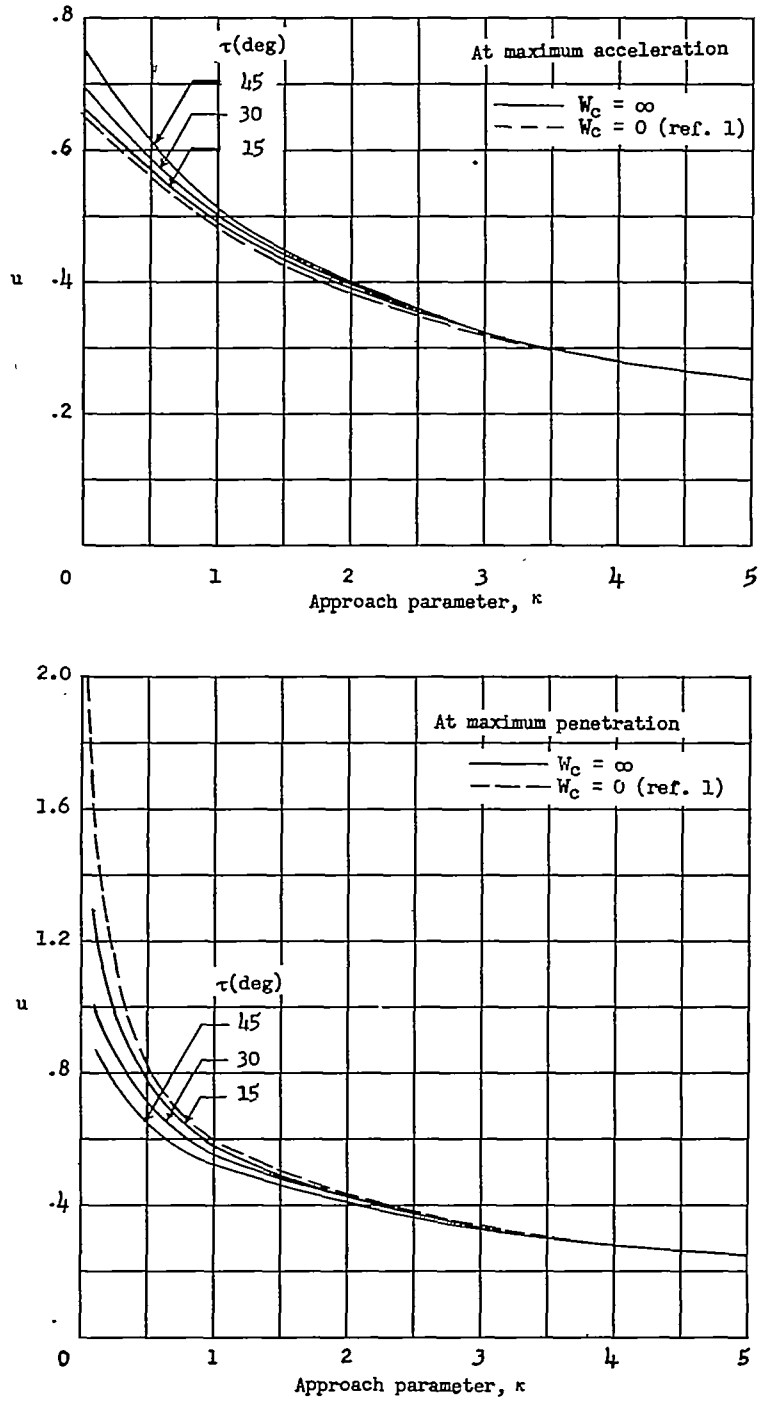

(a) Generalized displacement u.

Figure 10.- Comparison of theoretical variation of generalized variables at particular stages of impact with approach parameter for carriage masses of zero and infinity.

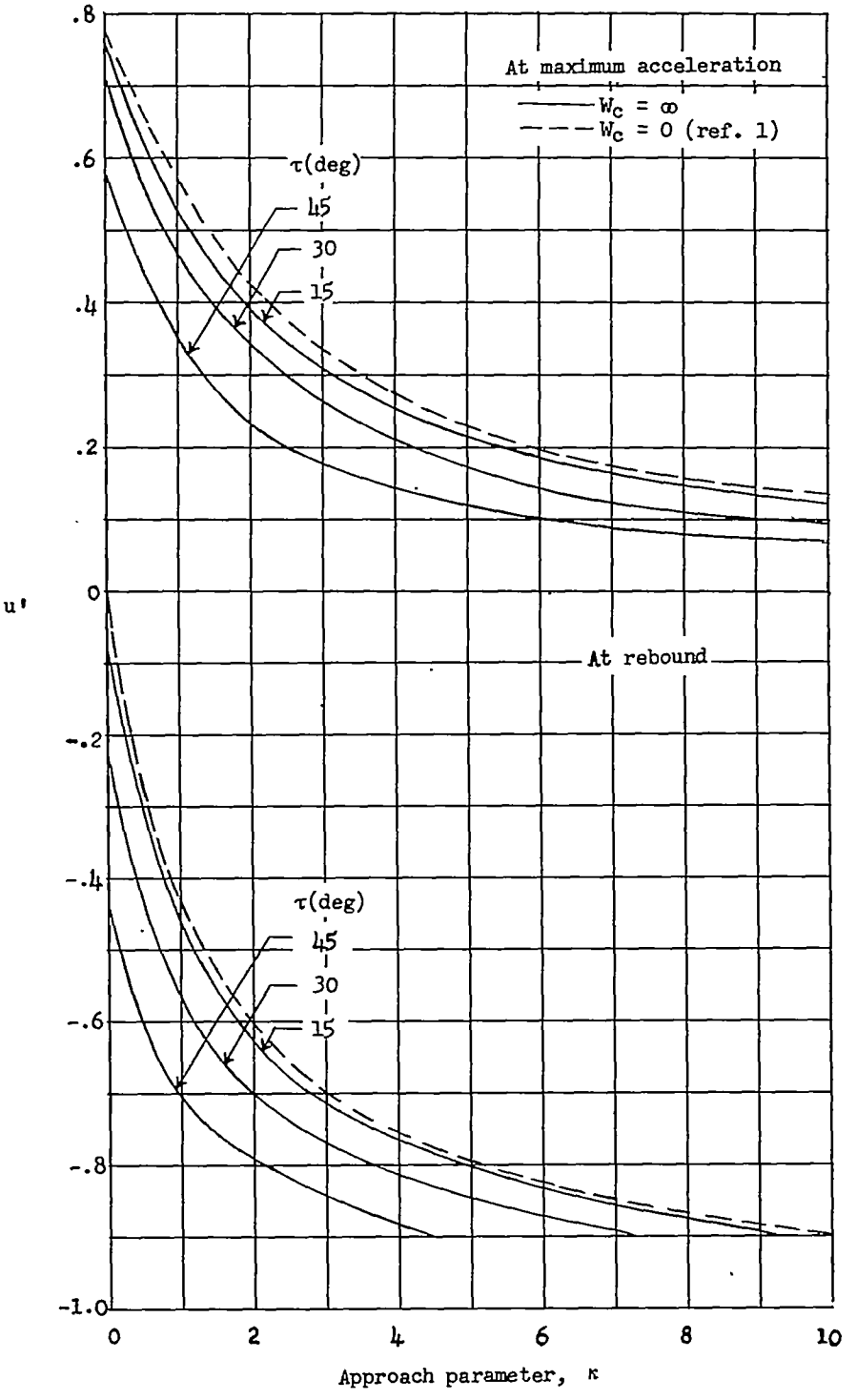

(b) Generalized velocity u'.

Figure 10.- Continued.

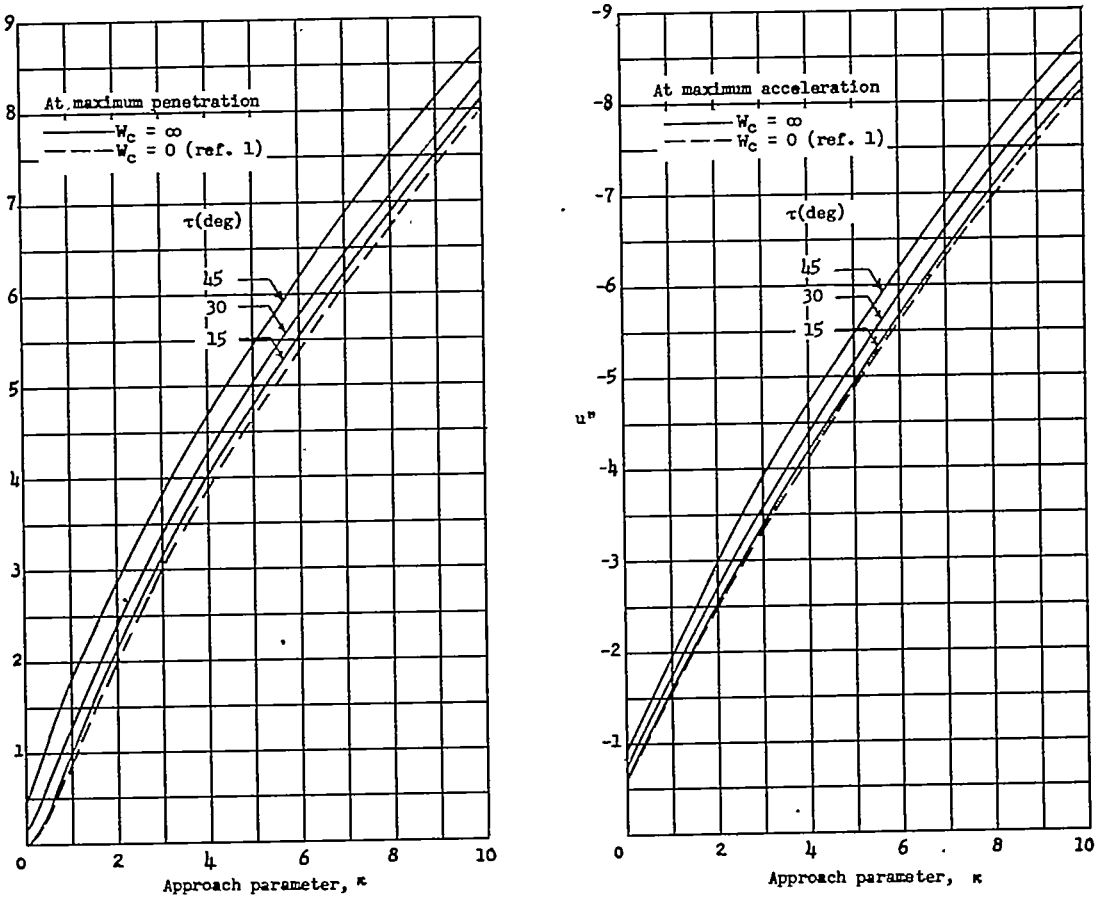

(c) Generalized acceleration u".

Figure 10.- Continued.

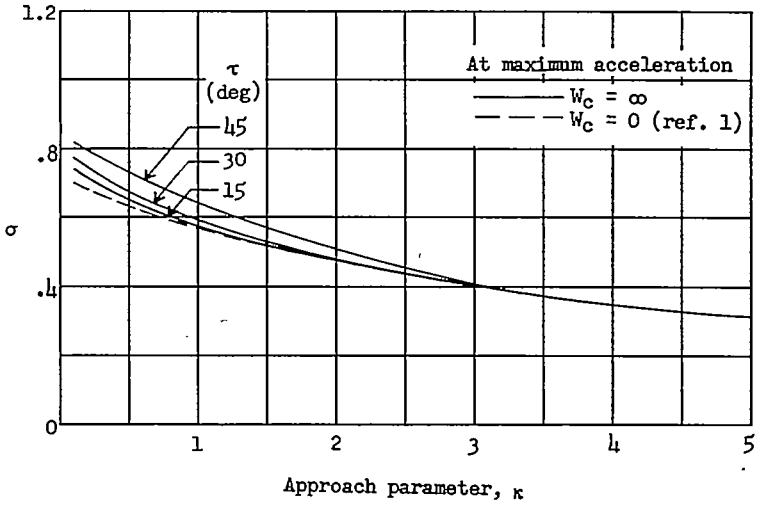

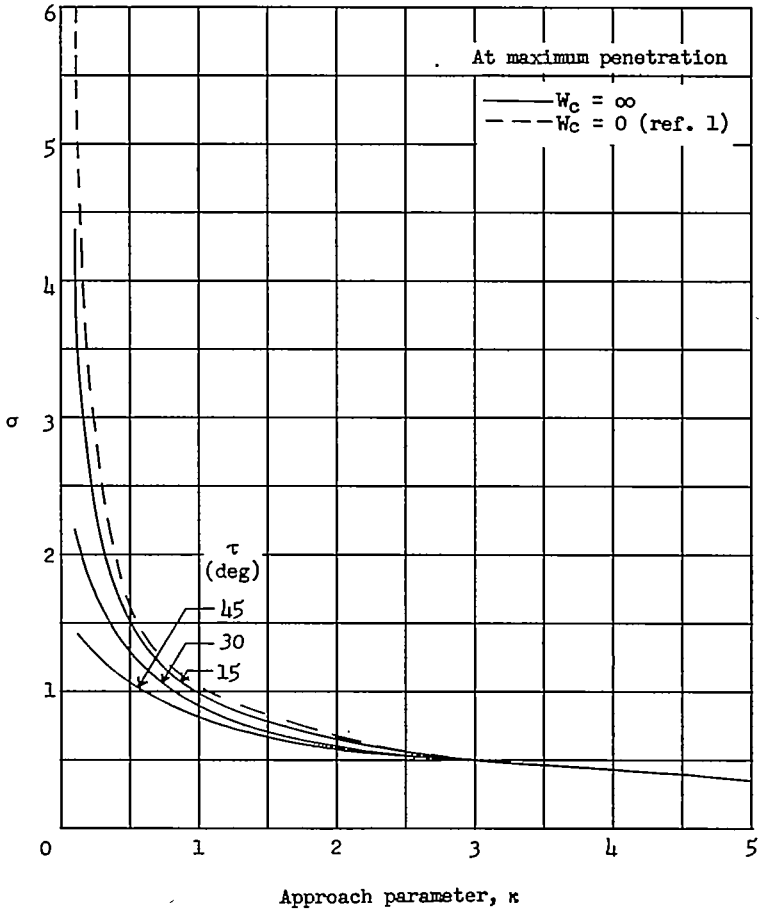

(d) Generalized time σ.

Figure 10.- Continued.

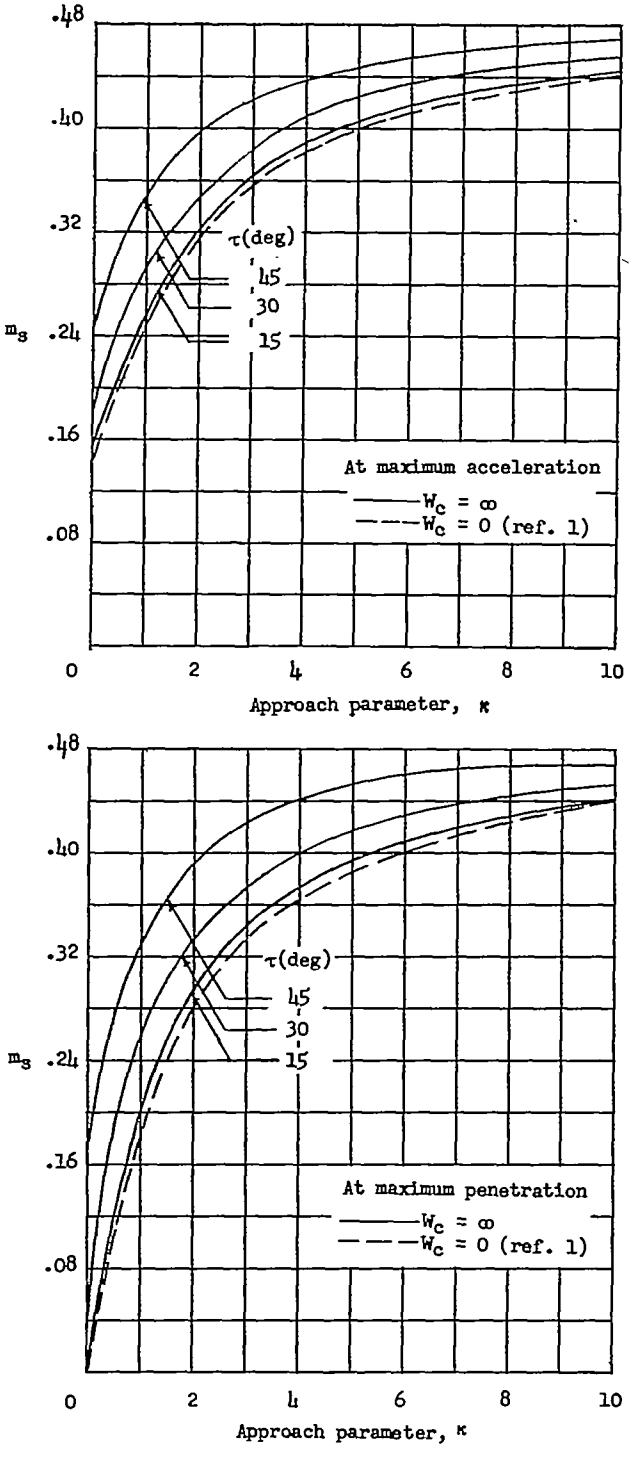

(e) Generalized pitching moment about step m_s.

Figure 10.- Continued.

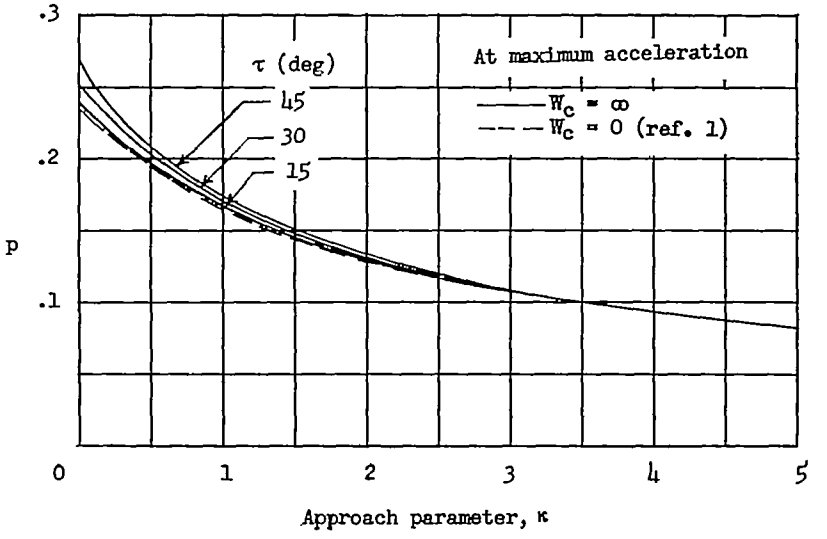

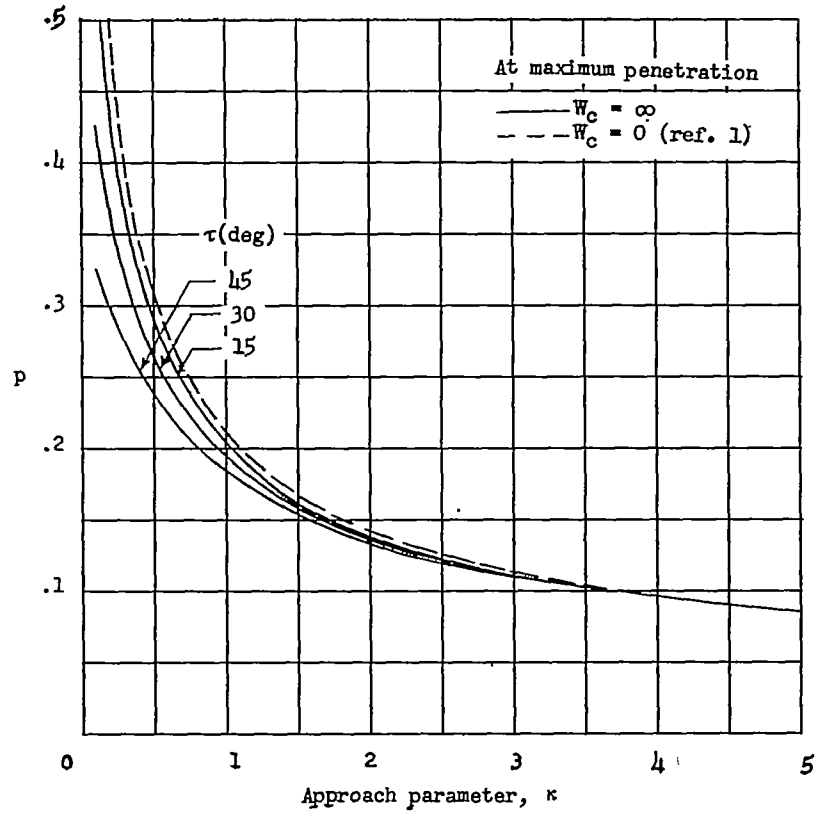

(f) Generalized center-of-pressure distance p.

Figure 10.- Concluded.

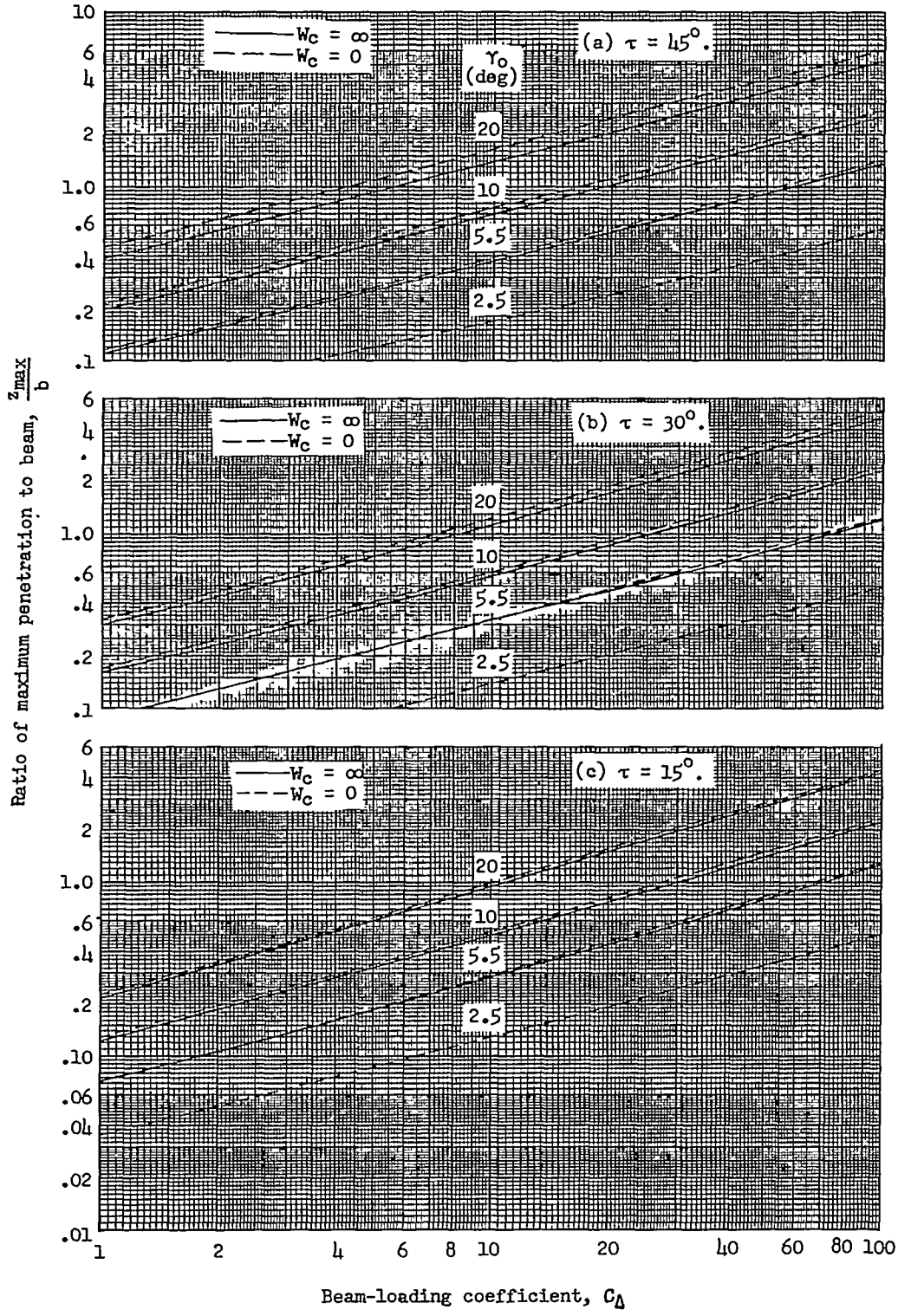

Figure 11.- Theoretical comparison of maximum penetration z/b_{max} of flat plates between zero and infinite carriage masses.

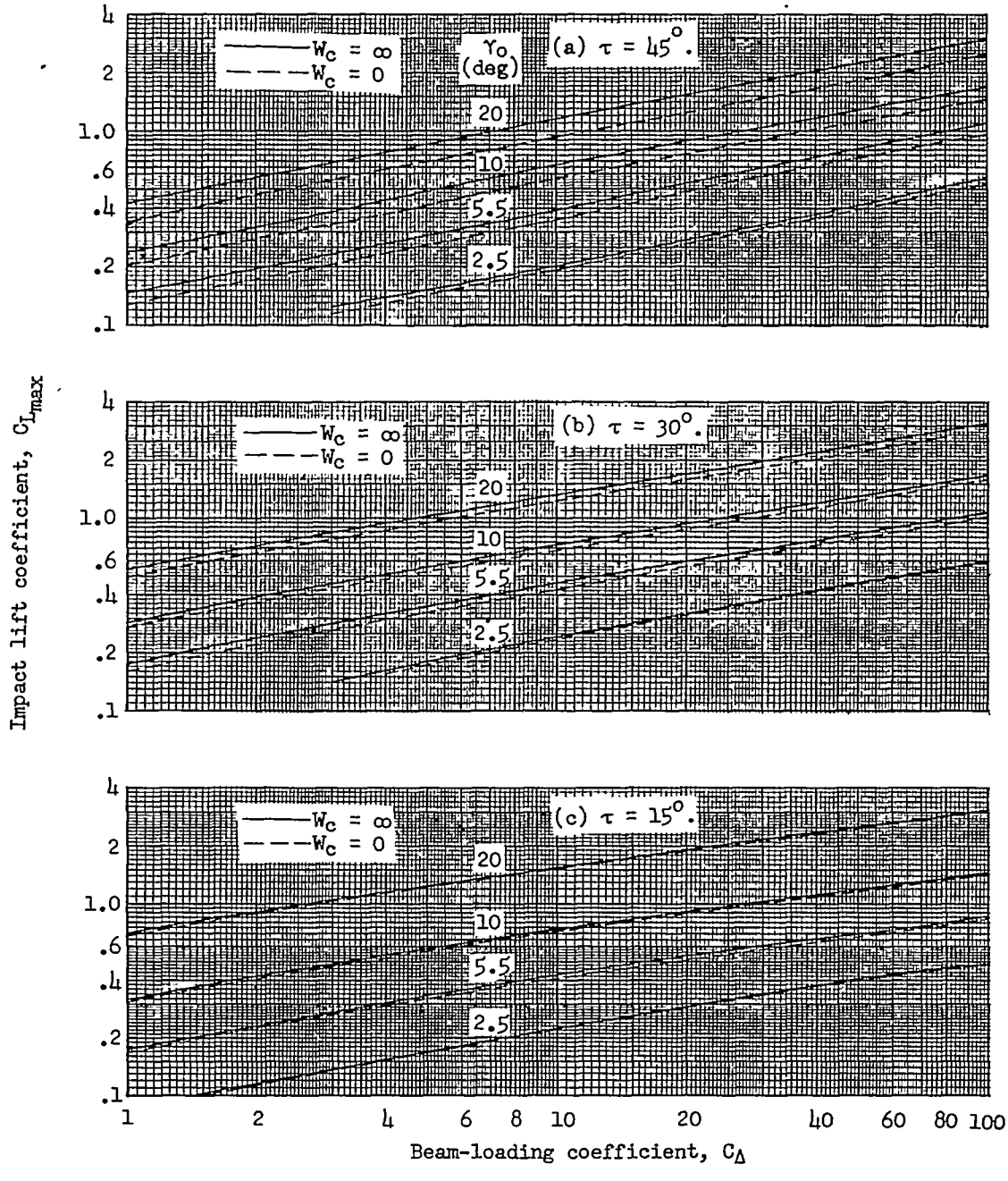

Figure 12.- Theoretical comparison of maximum impact lift coefficient $C_{L_{max}}$ of flat plates between zero and infinite carriage masses.